Delft University of Technology

Physics enhanced sparse identification of dynamical systems with discontinuous nonlinearities

Lathourakis, Christos; Cicirello, Alice

Important note
To cite this publication, please use the final published version (if applicable).
Please check the document version above.

Physics enhanced sparse identification of dynamical systems with discontinuous nonlinearities

Christos Lathourakis · Alice Cicirello

Abstract A method is introduced for the identification of the nonlinear governing equations of dynamical systems in the presence of discontinuous and nonsmooth nonlinear forces, such as the ones generated by frictional contacts, based on noisy measurements. The so-called Physics Encoded Sparse Identification of Nonlinear Dynamics (PhI-SINDy) builds upon the existing RK4-SINDy identification scheme, incorporating known physics and domain knowledge in three different ways (biases). In this way, it addresses the discontinuous behavior of frictional systems when stick–slip phenomena are observed, which can not be captured by existing state-of-the-art approaches. The potential of PhI-SINDy is highlighted through a plethora of case studies, starting from a simple yet representative Single Degree of Freedom (SDOF) oscillator with a Coulomb friction contact under harmonic load, using both synthetic and experimental noisy measurements. An alternative friction law, namely the Dieterich-Ruina one, is also considered as well as a more realistic excitation time series, which was gen-

erated based on the Jonswap spectrum. Lastly, a Multi Degree of Freedom system with single and multiple friction contacts is used as a testbed, showcasing the applicability of PhI-SINDy to more complicated systems and/or multiple sources of discontinuous nonlinearities.

1 Introduction

An ongoing problem in structural engineering is the characterization of friction damping in structural dynamics. Frictional joints appear in most applications and industries, including aerospace, automotive, and construction. However, the friction force identification is hindered by its discontinuous nature, which is responsible for the non-smooth response of engineering systems, and frequently leads to stick–slip phenomena. To this end, alternative constitutive laws have been suggested as a solution [1,2], and experimental data has been used to validate proposed friction models [2,3], [4].

The identification of the underlying differential equations of physical problems based on noisy observations has been rendered more feasible through the rapid growth in data availability and the recently developed tools for system identification. The identification

C. Lathourakis (✉) · A. Cicirello
Faculty of Civil Engineering and Geosciences, Delft University of Technology, Stevinweg 1, 2628 CN Delft, The Netherlands
e-mail: xristosl0610@gmail.com

A. Cicirello
e-mail: ac685@cam.ac.uk

A. Cicirello
Department of Engineering, University of Cambridge, Trumpington Street, Cambridge CB2 1PZ, UK

of smooth localized nonlinearities has already been carried out in [5–7] by using the promising framework known as Sparse Identification of Nonlinear Dynamics (SINDy), which was developed in [8]. Nevertheless, frictional problems may call for the discovery of discontinuous non-smooth physical laws, more often than not, based on sparse and noisy observations collected during stick–slip events [9]. An efficient way to treat such nonlinearities has been developed in [10] where a switching Gaussian Process Latent Force Model (GPLFM) is utilized, however, such an approach can not be extended to Multi Degree of Freedom (MDOF) systems with multiple nonlinearities in a straightforward manner. The use of stick and slip temporal constraints along with SINDy was explored in [11] to identify the governing equation of SDOF oscillators with friction, facing limitations though when it comes to more complex MDOF systems or when considerable noise levels intervened in the differentiation of measured data. A further enhancement of SINDy, known as RK4-SINDy, was presented in [12], where a numerical constraint, namely the 4th-order Runge–Kutta integration scheme, was implemented and demonstrated to more effectively handle noise in the data. This method was explored for the identification of friction regarding continuous motion in [13], pointing towards the need to further develop this approach to tackle stick–slip phenomena and MDOF systems.

An ever-important challenge when applying the aforementioned identification techniques is the generalization of the derived equation. Purely data-driven models may fit noisy observations adequately, however, extrapolation and the underlying observational biases often lead to inconsistent predictions, and in general, a poor generalization performance, as described thoroughly in [14]. Promising results were also produced in [15] when no prior knowledge about physics, kinematics, or geometry, was used, emphasizing on the other hand that the inclusion of physical laws accelerated the identification of complex systems. This is why, the inclusion of domain knowledge and/or physical laws in the employed identification techniques is a crucial issue, to produce explainable and generalizable governing equations.

The current paper introduces a modified version of RK4-SINDy, where physics biases are included. The Physics Encoded Sparse Identification of Nonlinear Dynamics (PhI-SINDy), is presented and its applicability to identify the governing equation of fric-

tional systems in the discontinuous motion regime is tested. A variety of case studies are explored, starting from a Single Degree of Freedom (SDOF) oscillator with a Coulomb friction contact under harmonic loading, using both synthetic and experimental noisy measurements. Additionally, a different friction law is accounted for, i.e. the Dieterich-Ruina (DR) model presented in [16,17], a more complex excitation, namely the Jonswap spectrum [18], and lastly an MDOF system with single and multiple friction contacts are explored.

2 Sparse identification with Runge–Kutta constraint (RK4-SINDy)—review

The goal of sparse identification is to identify a nonlinear model using the fewest terms possible to capture the temporal evolution of the measurement data. The so-called RK4-SINDy, a Runge-Kutta-inspired sparse identification approach, was proposed in [12] and focuses on determining the underlying nonlinear differential equations of dynamical systems from corrupted and/or sparsely gathered data. RK4-SINDy was formed by coupling sparse identification with a classical numerical integration tool, in particular, SINDy [8] was combined with the fourth-order Runge–Kutta integration scheme applied to a mathematical model of the physical system.

Let us consider an n-dimensional dynamical system that is described by the following equation:

$$\dot{\mathbf{x}}(t) = \frac{\mathrm{d}}{\mathrm{d}t}\mathbf{x}(t) = \mathbf{f}(\mathbf{x}(t), t) \qquad (1)$$

where the $n \times 1$ vector $\mathbf{x}(t) = \begin{bmatrix} x_1(t) \ x_2(t) \ \ldots \ x_n(t) \end{bmatrix}^{\mathrm{T}}$ corresponds to the system's state at time t, and the function $\mathbf{f}(\mathbf{x}(t)) : \mathbb{R}^n \to \mathbb{R}^n$ describes the functional relationship between $\mathbf{x}(t)$ and its derivatives. This $\mathbf{f}(\mathbf{x}(t))$ is often referred to as the vector field, in other words, the set of candidate functions that formulate the equations of motion of the system. A key observation made by [8] states that for many systems of interest, only a few terms are necessary to formulate $\mathbf{f}$, underlining its sparsity in the space of possible functions. Sparse regression facilitates the derivation of the non-zero terms contained in $\mathbf{f}$ without an exhausting brute-force search [8]. Hence, the sought vector fields can be expressed as the product of a dictionary of N candidate functions, $\boldsymbol{\theta}(\mathbf{x}(t))$, and a sparse matrix of coefficients, $\Xi = \begin{bmatrix} \boldsymbol{\xi}_1, \ \boldsymbol{\xi}_2, \ \ldots \ \boldsymbol{\xi}_n \end{bmatrix}$, that determines which features should be dropped and

which ones should be included in the final solution, and to what extent they contribute to it:

$$\mathbf{f}\big(\mathbf{x}(t)\big) = \Big[\boldsymbol{\theta}\big(\mathbf{x}(t)\big) \cdot \boldsymbol{\Xi}\Big]^{\mathrm{T}} \tag{2}$$

Each $\boldsymbol{\xi_i}$ is an $N \times 1$ vector, where N is the number of the assumed features of the $\boldsymbol{\theta}(\mathbf{x}(t))$ dictionary, and refers exclusively to the i-th state of $\mathbf{x}(t)$. Thus the dimensions of $\boldsymbol{\theta}(\mathbf{x}(t))$ and $\boldsymbol{\Xi}$ are $1 \times N$ and $N \times n$ respectively.

The dictionary of features, $\boldsymbol{\theta}(\mathbf{x}(x))$, can contain various nonlinear functions, e.g. polynomials, trigonometric, exponential, etc. For any given state vector $\mathbf{x}(t)$ it can take the following form:

$$\boldsymbol{\theta}\big(\mathbf{x}(t)\big) = \begin{bmatrix} 1 \\ \mathbf{x}(t) \\ \mathbf{x}^{\mathcal{P}_2}(t) \\ \mathbf{x}^{\mathcal{P}_3}(t) \\ \vdots \\ \cos(\mathbf{x}(t)) \\ \cos(2\,\mathbf{x}(t)) \\ \vdots \\ \mathrm{e}^{-\mathbf{x}(t)} \\ \vdots \end{bmatrix}^{\mathrm{T}} \tag{3}$$

in which, $\mathbf{x}^{\mathcal{P}_i}(t)$ denotes polynomials of the i-th order, for instance:

$$\mathbf{x}^{\mathcal{P}_2} = \begin{bmatrix} x_1^2(t) \\ x_1(t)x_2(t) \\ \vdots \\ x_1(t)x_n(t) \\ x_2^2(t) \\ x_2(t)x_3(t) \\ \vdots \\ x_{n-1}(t)x_n(t) \\ x_n^2(t) \end{bmatrix}^{\mathrm{T}} \tag{4}$$

It is essential to note the training data evolution over time may be accurately described by the use of polynomials. However, since the terms of the equation will not be generalizable, this could result in overfitting, hence, in poor predictions when a new dataset is employed, as shown in [13].

The coefficients in each sparse column vector $\boldsymbol{\xi}_j$ act as weights for the candidate features that should be included in the right-hand side for the equation $\dot{x}_j = f_j(\mathbf{x}(t))$. $\boldsymbol{\Xi}$ is determined through a nonlinear and likely non-convex optimization leading to a sparse solution. This requires defining an appropriate loss function, usually including a sparsity-promoting parameter. Finally, each equation of the unknown vector field is:

$$\dot{x}_j(t) = f_j(\mathbf{x}(t)) = \boldsymbol{\theta}(\mathbf{x}(t)) \cdot \boldsymbol{\xi}_j \tag{5}$$

Considering discrete time instances t_k, $k = 1, 2, \ldots, m$, the following matrix is formed, which contains the state vector $\mathbf{x}(t)$ at different times:

$$\mathbf{X} = \begin{bmatrix} \mathbf{x}^{\mathrm{T}}(t_1) \\ \mathbf{x}^{\mathrm{T}}(t_2) \\ \vdots \\ \mathbf{x}^{\mathrm{T}}(t_m) \end{bmatrix} = \begin{bmatrix} x_1(t_1) & x_2(t_1) & \cdots & x_n(t_1) \\ x_1(t_2) & x_2(t_2) & \cdots & x_n(t_2) \\ \vdots & \vdots & \ddots & \vdots \\ x_1(t_m) & x_2(t_m) & \cdots & x_n(t_m) \end{bmatrix} \tag{6}$$

The column entries of $\mathbf{X}$ can also be interpreted as time series of the individual state variables, $x_j(t_k)$, $k = 1, 2, \ldots, m$.

The feature library $\boldsymbol{\theta}(\mathbf{x}(t))$ can now be re-written as a matrix:

$$\boldsymbol{\Theta}(\mathbf{X}) = \begin{bmatrix} \boldsymbol{\theta}(\mathbf{x}(t_1)) \\ \boldsymbol{\theta}(\mathbf{x}(t_2)) \\ \vdots \\ \boldsymbol{\theta}(\mathbf{x}(t_m)) \end{bmatrix} \tag{7}$$

transforming also Eq. (2) into:

$$\dot{\mathbf{X}} = \Big[\boldsymbol{\Theta}(\mathbf{X}) \cdot \boldsymbol{\Xi}\Big]^{\mathrm{T}} \tag{8}$$

Within the RK4-SINDy [12], the Runge–Kutta scheme is used to relate the measurement at t_{k+1} with the previous one at t_k via:

$$\mathbf{x}(t_{k+1}) = \mathbf{x}(t_k) + \int_{t_k}^{t_{k+1}} \mathbf{f}(\mathbf{x}(\tau))\mathrm{d}\tau \tag{9}$$

Therefore, reducing the solution space, such that:

$$\mathbf{x}(t_{k+1}) \approx \mathbf{RK4}(\mathbf{f}(\mathbf{x}(t_k)), \mathbf{x}(t_k), h_k) \tag{10}$$

where $\mathbf{RK4}$ indicates:

$$\mathbf{RK4}(\mathbf{f}(\mathbf{x}(t_k)), \mathbf{x}(t_k), h_k) = \mathbf{x}(t_k) \\ + \frac{1}{6}h_k\,(\mathbf{k}_1 + 2 \cdot \mathbf{k}_2 + 2 \cdot \mathbf{k}_3 + \mathbf{k}_4), \quad h_k = t_{k+1} - t_k \tag{11}$$

where

$$\mathbf{k}_1 = \mathbf{f}\,(\mathbf{x}\,(t_k)) \qquad \mathbf{k}_2 = \mathbf{f}\left(\mathbf{x}\,(t_k) + h_k\frac{\mathbf{k}_1}{2}\right)$$

$$\mathbf{k}_3 = \mathbf{f}\left(\mathbf{x}\,(t_k) + h_k\frac{\mathbf{k}_2}{2}\right) \qquad \mathbf{k}_4 = \mathbf{f}\,(\mathbf{x}\,(t_k) + h_k\mathbf{k}_3)$$

$$\tag{12}$$

The RK4 scheme can propagate also backward in time, using a negative time step h_k, meaning that predictions both for $\mathbf{x}(t_{k+1})$ and $\mathbf{x}(t_{k-1})$ can be made.

A loss function, $\mathcal{L}$, needs to be formulated to determine the optimal matrix of coefficients, Ξ. This can be the Mean Squared Error or any other loss criterion, that considers the similarity between the measurements, $\mathbf{X}^*$ and the obtained predictions through Eq. (10), $\mathbf{X}^{\text{pred}}$:

$$\underset{\Xi}{\text{argmin}} \; \mathcal{L}\left(\mathbf{X}^*, \mathbf{X}^{\text{pred}}\right) \tag{13}$$

To arrive at a parsimonious solution that will not include redundant terms, the promotion of sparsity is necessary, through an l_1-regularization term:

$$\underset{\Xi}{\text{argmin}} \; \mathcal{L}\left(\mathbf{X}^*, \mathbf{X}^{\text{pred}}\right) + \alpha \; || \; \Xi \; ||_{l_1} \tag{14}$$

where α is a regularizing parameter.

However, as noted in [12], the optimization problem denoted by Eq. (14) is not convex, making it inefficient to employ conventional methods for linear optimization problems, such as LASSO [19,20]. Hence, the fixed cut-off thresholding algorithm, introduced in [12], is used with minor adjustments also for the current work. To be more precise, the Stochastic Gradient Descent (SGD) method is used to update the ξ coefficients to minimize the mismatch between measurements and predictions. In this procedure, a cut-off value λ is selected, and after each passing of the measurements (a single time series, which ideally includes both transient and steady-state responses, to provide more information which might improve the accuracy of the sparse identification), all the coefficients whose absolute values are less than λ are set to zero, proceeding with the non-zero ones to the subsequent iteration. In Algorithm 1 the exact step-by-step procedure is described.

The choice of the cut-off value is a disadvantage of such a method. In an ideal scenario, an iterative process is required in which several values of λ are selected and their respective performances are assessed.

3 Physics encoded RK4-SINDy - PhI-SINDy for dynamical systems with discontinuous nonlinearities

In [12] it was indicated that finding governing equations may be made considerably more effective when physics knowledge was included, however, it was not

---

Algorithm 1 Fixed Cut-off Thresholding

Input: Measurement data $\mathbf{X}^*$, Feature dictionary $\boldsymbol{\theta}(\mathbf{x}(t))$, Cutoff parameter λ,
Number of training epochs M
1: Initialize coefficient matrix Ξ with 0 values
2: **for** $i \leftarrow 1$ **to** M **do**
3:     $\mathbf{X}^{\text{pred}} \leftarrow \mathbf{RK4}\left(\Theta(\mathbf{X}) \cdot \Xi, \mathbf{X}^*\right)$
4:     Solve
$$\underset{\Xi}{\text{argmin}} \; \mathcal{L}\left(\mathbf{X}^*, \mathbf{X}^{\text{pred}}\right)$$
    using SGD
5:     $inds = | \; \Xi \; | < \lambda$ ▷ The indices of the coefficients
6:                                  smaller than λ
7:     $\Xi[inds] \leftarrow 0$
Output: The sparse coefficient matrix Ξ

---

further investigated. This is especially crucial when discontinuous nonlinearities are present in dynamical systems because state-of-the-art identification techniques cannot effectively capture them. A more generalizable solution would be produced by using physics, especially in situations with limited data availability. Incorporating physics might resolve overfitting concerns (which consequently diminish the predictive power of the resultant governing equation) seen with solely data-driven systems when conducting the identification using noisy and/or sparse data. Elaborating on the thorough review of physics-informed machine learning by [14] there are four different methods that can be used to add physics knowledge:

- **Observational bias:**
  Provide training data that obey the underlying physics and/or using advanced data augmentation procedures
- **Learning bias:**
  Include loss functions, optimization constraints, and inference algorithms that facilitate the convergence toward the underlying physics
- **Inductive bias:**
  Modify the algorithm architecture, by incorporating prior assumptions and physical constraints
- **Model form/discrepancy bias:**
  Incorporate known terms describing the partially known physics-based model

In the current work, PhI-SINDy is introduced to tackle the more general case of identifying the nonlinear differential equations of a non-autonomous system in the presence of discontinuous nonlinearities by including three of the four biases mentioned above. Applying this physics-enhanced framework to noisy

measurements, the sought differential equations are derived in a deterministic fashion.

A **discrepancy bias** is introduced by decomposing the set of governing equations into a known part and a part that needs to be identified.

$$\dot{\mathbf{x}}(t) = \underbrace{\mathbf{f}(t, \mathbf{x}(t))}_{\substack{\text{part to be} \\ \text{identified}}} + \underbrace{\mathbf{g}(t, \mathbf{x}(t))}_{\text{known part}} \qquad (15)$$

The vector $\mathbf{g}(t, \mathbf{x}(t))$ is deterministic, known beforehand, and provided in a hardcoded manner for the derived solution. Particular care must be taken when setting this bias since providing the wrong physics can lead to inaccuracies regarding the identified vector fields, as showcased in [13]. The $\mathbf{f}(t, \mathbf{x}(t))$ vector, i.e. the part of the equation to be identified, is expressed as shown in Eq. (2). In other words, Eq. (15) assumes that the functional form of the part of the equation to be identified and its parameters are deterministic but unknown because of lack of knowledge (epistemic uncertainty), while other forms of uncertainty (e.g. parameter uncertainty, noise uncertainty, and other aleatoric uncertainties) are not accounted for.

The solution provided by RK4-SINDy relies on the initial assumption of the candidate functions, as summarised in Sect. 2. This decision along with the fact that, for the sake of sparsity, terms whose contribution is minor to the final solution are dropped, shrink the solution space, and act as constraints to the identified governing equation. Such aspects of the method can be interpreted as an **inductive bias** that shifts the end results according to user-provided information. Setting this bias requires special attention since an uneducated choice of these factors might produce an accurate result with low generalizability, for instance when only linear polynomial functions are considered, as shown in [13]. Moreover, in the case of dynamical systems that include discontinuous behavior (such as a system with friction where stick–slip phenomena occur) or that are described by stiff governing equations, it is essential to include an event condition in the learning process, which will handle measurements that comply with this condition in a different manner. This necessity emerges from the fact that the sought differential equations usually refer to continuous motion described by smooth functions, while the available measurements might exhibit also discontinuous and non-smooth trends. This physical constraint, which acts as an additional inductive bias, is defined as $c(\mathbf{x}^*(t_k)) = 0, \ k = 1, \ldots, m$.

Lastly, a **learning bias** is introduced by modifying the learning algorithm, specifically by modifying Eqs. (9)–(12) to explicitly account for the known physics and the physical constraints:

$$\mathbf{x}(t_{k+1}) = \mathbf{x}(t_k) + \int_{t_k}^{t_{k+1}} \Big(\mathbf{f}(\tau, \mathbf{x}(\tau)) + \mathbf{g}(\tau, \mathbf{x}(\tau)) \Big) d\tau \qquad (16)$$

$$\mathbf{x}(t_{k+1}) \approx \mathbf{RK4}(\mathbf{f}(t_k, \mathbf{x}(t_k)), \mathbf{g}(t_k, \mathbf{x}(t_k)), \\ c(\mathbf{x}(t_k)), \mathbf{x}(t_k), h_k) \qquad (17)$$

$$\mathbf{RK4}(\mathbf{f}(t_k, \mathbf{x}(t_k)), \mathbf{g}(t_k, \mathbf{x}(t_k)), c(\mathbf{x}(t_k)), \mathbf{x}(t_k), h_k) \\ = \mathbf{x}(t_k) + \frac{1}{6} h_k (\mathbf{k}_1 + 2 \cdot \mathbf{k}_2 + 2 \cdot \mathbf{k}_3 + \mathbf{k}_4) \qquad (18)$$

where

$$\mathbf{k}_1 = \mathbf{f}(t_k, \mathbf{x}(t_k)) + \mathbf{g}(t_k, \mathbf{x}(t_k))$$
$$\mathbf{k}_2 = \mathbf{f}\left(t_k, \mathbf{x}(t_k) + h_k \frac{\mathbf{k}_1}{2}\right) + \mathbf{g}\left(t_k, \mathbf{x}(t_k) + h_k \frac{\mathbf{k}_1}{2}\right)$$
$$\mathbf{k}_3 = \mathbf{f}\left(t_k, \mathbf{x}(t_k) + h_k \frac{\mathbf{k}_2}{2}\right) + \mathbf{g}\left(t_k, \mathbf{x}(t_k) + h_k \frac{\mathbf{k}_2}{2}\right)$$
$$\mathbf{k}_4 = \mathbf{f}(t_k, \mathbf{x}(t_k) + h_k \mathbf{k}_3) + \mathbf{g}(t_k, \mathbf{x}(t_k) + h_k \mathbf{k}_3) \qquad (19)$$

It should be noted that the known physics and the physical constraint can be applied to both vectors and matrices of measurements, $\mathbf{g}(t, \mathbf{x}(t))$, $c(\mathbf{x}(t))$ and $\mathbf{G}(\mathbf{t}, \mathbf{X})$, $c(\mathbf{X})$, respectively, with the following transformation in their dimensions.

$$\mathbf{g}(t, \mathbf{x}(t)) = \begin{bmatrix} g_1(t, \mathbf{x}(t)) \\ g_2(t, \mathbf{x}(t)) \\ \vdots \\ g_n(t, \mathbf{x}(t)) \end{bmatrix} \qquad (20)$$

$$\mathbf{G}(\mathbf{t}, \mathbf{X}) = \begin{bmatrix} \mathbf{g}^{\mathrm{T}}(t_1, \mathbf{x}(t_1)) \\ \mathbf{g}^{\mathrm{T}}(t_2, \mathbf{x}(t_2)) \\ \vdots \\ \mathbf{g}^{\mathrm{T}}(t_m, \mathbf{x}(t_m)) \end{bmatrix}$$
$$= \begin{bmatrix} g_1(t_1, \mathbf{x}(t_1)) & g_2(t_1, \mathbf{x}(t_1)) & \cdots & g_n(t_1, \mathbf{x}(t_1)) \\ g_1(t_2, \mathbf{x}(t_2)) & g_2(t_2, \mathbf{x}(t_2)) & \cdots & g_n(t_2, \mathbf{x}(t_2)) \\ \vdots & \vdots & \ddots & \vdots \\ g_1(t_m, \mathbf{x}(t_m)) & g_2(t_m, \mathbf{x}(t_m)) & \cdots & g_n(t_m, \mathbf{x}(t_m)) \end{bmatrix} \qquad (21)$$

$$\mathbf{c}(\mathbf{X}) = \begin{bmatrix} c(\mathbf{x}(t_1)) \\ c(\mathbf{x}(t_2)) \\ \vdots \\ c(\mathbf{x}(t_m)) \end{bmatrix} \qquad (22)$$

The complete step-by-step framework is presented in Algorithm 2.

Algorithm 2 PhI-SINDy learning algorithm

Input: Measurement data $\mathbf{X}^*$, ▷ A single time series of inputs and outputs

Known physics $\mathbf{g}(t, \mathbf{x}(t))$, ▷ Discrepancy bias

Feature dictionary $\boldsymbol{\theta}(\mathbf{x}(t))$, ▷ Inductive bias

Physical constraint $c(\mathbf{x}(t))$, ▷ Inductive bias

Cutoff parameter λ, Number of training epochs M ▷ Training hyperparameters

1: Initialize coefficient matrix Ξ with 0 values

2: **for** $i \leftarrow 1$ **to** M **do**

3:   $\mathbf{X}^{\text{pred}} \leftarrow \mathbf{RK4}\left(\Theta(\mathbf{X}) \cdot \Xi, \mathbf{G}(\mathbf{t}, \mathbf{X}^*), \mathbf{c}(\mathbf{X}^*), \mathbf{X}^*\right)$

      ▷ Learning bias

4:   Solve

$$\underset{\Xi}{\text{argmin}}\ \mathcal{L}\left(\mathbf{X}^*, \mathbf{X}^{\text{pred}}\right)$$

    using SGD

5:   $inds =| \Xi |< \lambda$ ▷ The indices of the coefficients

6:                      smaller than λ

7:   $\Xi[inds] \leftarrow 0$

Output: The sparse coefficient matrix Ξ

It is worth mentioning that instead of a learning bias, i.e. incorporating the event condition in the learning process, filtering of the data might be considered, therefore introducing an observational bias. For example, prior to the learning part of the algorithm, a segregation of the initial data, $\mathbf{X}^*$, could be carried out, as performed in [11], discarding the measurements that correspond to discontinuities.

$$\mathbf{X}^*_{\text{filt}} = \left\{\mathbf{X}^* \mid \mathbf{c}(\mathbf{X}^*) = \mathbf{0}\right\} \tag{23}$$

However, the calculation of the four intermediate derivatives within the RK4 scheme (Eq. (19)) would render the process unstable, since these intermediate points, $\mathbf{x}(t_k) + h_k \dfrac{\mathbf{k}_i}{2}$, need to be included in the learning process even if they refer to discontinuous parts of the motion.

The accuracy of the part to be identified especially of a nonlinear discontinuous term depends on the choice of measurement variables, the sampling frequency of the measurements, the known part of the equation, physical constraints, and candidate functions used to sparsely represent the dynamics. Unfortunately, depending on the application, it might be difficult to know in advance how to make these selections. Moreover, the presence of noise in the measurements as well as other confounding sources may affect the uniqueness of the identified sparse terms. These problems are discussed in Sect. 4 for a specific application. Moreover, recommendations on pre-processing, choosing the learning architecture, and validation are provided in Sect. 5. Lastly, it should be noted that the current formulation does not account for uncertainties in the

Table 1 Case studies investigated

Case ID	System	Type of motion	Friction law	Excitation
1a	Synthetic SDOF	Stick-slip (2 stops)	Coulomb	Harmonic
1b	Synthetic SDOF	Stick-slip (2 stops)	Dieterich-Ruina (DR)	Harmonic
2a	Synthetic SDOF	Stick-slip (4 stops)	Coulomb	Harmonic
2b	Synthetic SDOF	Stick-slip (4 stops)	DR	Harmonic
3	Synthetic SDOF	Stick-slip (2 stops)	Coulomb/DR	Harmonic
4	Synthetic SDOF	Stick-slip	Coulomb	Jonswap spectrum
5	Synthetic MDOF one nonlinearity	Stick-slip	Coulomb	Harmonic
6	Synthetic MDOF two nonlinearities	Stick-slip	Coulomb + Coulomb	Harmonic
7	Synthetic MDOF two nonlinearities	Stick-slip	Coulomb + DR	Harmonic
8	Experimental SDOF	Continuous	Coulomb	Harmonic
9a	Experimental SDOF	Stick-slip (2 stops)	Coulomb	Harmonic
9b	Experimental SDOF	Stick-slip (2 stops)	Dieterich-Ruina (DR)	Harmonic
10	Experimental SDOF	Stick-slip (4 stops)	Coulomb	Harmonic

parameters of the governing equations - nor for the known part or for the part to be identified.

4 Applicability of PhI-SINDy to friction problems

PhI-SINDy will be applied to both synthetic and experimental cases. Although experimental results are available only for a SDOF oscillator, the applicability of PhI-SINDy is explored also in MDOF systems when it comes to synthetic cases. To present the different case studies and the corresponding results in a streamlined manner, they are numbered and summarized in Table 1.

4.1 Synthetic cases

4.1.1 Single degree of freedom (SDOF) oscillator

Consider a SDOF oscillator, as illustrated in Fig. 1, which consists of a mass m, a spring of stiffness k, and a dashpot with a viscous damping coefficient c. An external forcing $F(t)$ is applied to the mass, while a nonlinear friction force F_{fr} is generated through its contact with a fixed wall. Such a system's Equation of Motion (EoM) is:

$$m\,\ddot{x}(t) + c\,\dot{x}(t) + k\,x(t) + F_{\text{fr}}(t) = F(t) \qquad (24)$$

$$\Rightarrow \ddot{x}(t) + 2\,\zeta\,\omega_n\,\dot{x}(t) + \omega_n^2\,x(t) + \frac{F_{\text{fr}}(t)}{m} = \frac{F(t)}{m} \qquad (25)$$

where $\zeta = c/(2\sqrt{k\,m})$ is the damping ratio, and $\omega_n = \sqrt{\dfrac{k}{m}}$ the natural frequency.

By using the state-space representation of Eq. (25) a coupled system of first-order differential equations is derived:

$$\begin{cases} \dot{x}(t) = y(t) \\ \dot{y}(t) = -2\,\zeta\,\omega_n y(t) - \omega_n^2\,x(t) - \dfrac{F_{\text{fr}}(t)}{m} + \dfrac{F(t)}{m} \end{cases} \qquad (26)$$

As a first case study, a monochromatic loading is considered, of the following form:

$$F(t) = F_0\,\cos(\Omega\,t) \qquad (27)$$

Regarding the discontinuous friction term, this is generically written as:

$$F_{\text{fr}}(t) = \gamma(\dot{x}(t))\,\text{sgn}(\dot{x}(t)) \qquad (28)$$
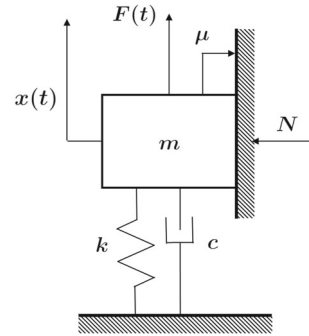
Fig. 1 SDOF schematic representation with $\gamma(\dot{x}(t)) = \mu N$

where the term $\gamma(\dot{x}(t))$ is defined according to the selected friction law and the signum function, $\text{sgn}(\dot{x})$, is defined as:

$$\begin{cases} 1 & \text{if } \dot{x} > 0 \\ [-1, 1] & \text{if } \dot{x} = 0 \\ -1 & \text{if } \dot{x} < 0 \end{cases} \qquad (29)$$

Taking into consideration these assumptions for the forcing and friction terms, the EoM, i.e. Eq. (26), takes the following form:

$$\dot{y}(t) = -2\,\zeta\,\omega_n y(t) - \omega_n^2\,x(t) - \frac{\gamma(y(t))}{m}\,\text{sgn}(y(t))$$
$$+ \frac{F_0}{m}\,\cos(\Omega\,t) \qquad (30)$$

There are two distinct phases in the motion of the oscillator, namely continuous motion and stick–slip. A continuous (smooth) motion of the mass, which is described by Eq. (30), is observed when the velocity is non-zero and the difference between the forcing and the spring force is greater than the friction force. On the other hand, stick phenomena occur when the velocity of the mass is zero, and the friction force is so dominant that counter-balances the rest of the forces acting on the mass. Thus the sticking condition can be formulated as follows:

$$\begin{cases} \dot{x}(t) = 0 \\ |F(t) - k\,x(t)| \leq |F_{\text{fr}}(t)| \end{cases} \qquad (31)$$

During stick–slip, the friction force is equal to the static friction:

$$F_{\text{fr, static}}(t) = F(t) - k\,x(t) \qquad (32)$$

Owing to its non-smooth nature, this type of problem is often referred to as stiff, meaning that standard integration methods perform poorly. To this end, the

Table 2 SDOF oscillator general properties

Quantity	Description	Value	Units
m	Mass	1	kg
c	Viscous damping coefficient	0.1	Ns/m
k	Stiffness	1	N/m
F_0	Forcing amplitude	1	N
Ω	Forcing frequency (2 stops per cycle)	0.3	rad/s
Ω	Forcing frequency (4 stops per cycle)	0.15	rad/s
x_0	Initial displacement (at $t = 0$)	0.1	m
$\dot{x}_0$	Initial velocity (at $t = 0$)	0.1	m/s

event condition of Eq. (31) is included explicitly in the Runge–Kutta method of order 5(4), to account for the transition between the sticking and the sliding regimes.

It should be noted that the latter of the two conditions in Eq. (31) is sensitive to noise, and enforcing it in the presence of noisy measurements might lead to wrong characterizations of the oscillator's motion. Thus, the physics constraints reduce to:

$$c(\mathbf{x}(t)) = \dot{x}(t) = 0 \tag{33}$$

The friction-to-forcing ratio and the ratio of the excitation frequency over the natural one are the parameters that dictate whether the oscillator will follow a smooth continuous motion or stick–slip phenomena will be observed. More information regarding these two quantities and their values in the case of stick–slip is provided in [21]. In the current work, two different forcing frequencies are considered, which will result in stick–slip motion with two and four stops per cycle.

The system properties, which are present in Eq. (30), are summarized in Table 2.

The values above are used to generate the displacement and velocity time histories, $\mathbf{X}_{\text{true}}$, with the explicit Runge-Kutta method of order 5(4) [22], which are then contaminated with noise, according to Eq. (34) to yield the noisy data given as input to PhI-SINDy.

$$\mathbf{X}^* \sim \mathcal{N}(\mathbf{X}_{\text{true}}, \sigma_{\text{noise}} \cdot \mathbf{X}_{\text{true}}) \tag{34}$$

In other words each entry of $\mathbf{X}^*$ (displacement and velocity time series) is contaminated by an independent zero mean Gaussian distribution with standard deviation σ_{noise}.

It should be mentioned that in [13], various noise levels were examined for the continuous motion of a synthetic SDOF oscillator. The worst-case scenario

of those cases is considered in the current work, i.e. $\sigma_{\text{noise}} = 10\%$.

Taking into consideration the aforementioned assumptions and rewriting Eq. (26) using matrix notation, it holds:

$$\mathbf{x}(t) = \begin{bmatrix} x(t) \\ y(t) \end{bmatrix} \tag{35}$$

$$\begin{bmatrix} \dot{x}(t) \\ \dot{y}(t) \end{bmatrix} = \begin{bmatrix} 0 & 1 \\ -\omega_n^2 & -2\,\zeta\,\omega_n \end{bmatrix} \cdot \begin{bmatrix} x(t) \\ y(t) \end{bmatrix} + \begin{bmatrix} 0 \\ \dfrac{F(t)}{m} \end{bmatrix}$$

$$- \begin{bmatrix} 0 \\ \dfrac{F_{\text{fr}}(t)}{m} \end{bmatrix}$$

$$\Rightarrow \frac{\mathrm{d}}{\mathrm{d}t}\mathbf{x}(t)$$

$$= \underbrace{\begin{bmatrix} 0 & 1 \\ -\omega_n^2 & -2\,\zeta\,\omega_n \end{bmatrix} \cdot \mathbf{x}(t) + \begin{bmatrix} 0 \\ \dfrac{F_0}{m}\cos(\Omega\,t) \end{bmatrix}}_{\text{known physics, } \mathbf{g}(t, \mathbf{x}(t))}$$

$$- \underbrace{\begin{bmatrix} 0 & 0 \\ 0 & \dfrac{\gamma(y(t))}{m} \end{bmatrix} \cdot \text{sgn}(\mathbf{x}(t))}_{\substack{\text{part to be} \\ \text{identified, } \mathbf{f}(t, \mathbf{x}(t))}} \tag{36}$$

In this paper it is assumed that the system parameters in the known physics part are deterministic, even though in more complex applications the damping value might be highly uncertain.

In what follows (apart from case 8), the dependency of the friction force on the moving direction of the mass, i.e. the sign of the velocity, is considered as part of the known physics (inductive bias), therefore the signum function is always explicitly defined independently of the friction model assumed. Thus, the candidate features, weighted by $\boldsymbol{\Xi}$ as explained in Sect. 2, are then multiplied by $\text{sgn}(y(t))$ aiming to identify the $\gamma(y(t))/m$ coefficient accurately. The final identified vector field is formulated as:

$$\mathbf{f}(t, \mathbf{x}(t)) = \left[\boldsymbol{\theta}(x, y) \cdot \boldsymbol{\Xi} \cdot \text{sgn}(y(t)) \right]^{\mathrm{T}} \tag{37}$$

The loss function chosen for the cases explored in the current work is the Mean Squared Error (MSE) between the RK4 predictions and the measurements.

4.1.1.1 Case 1: Two stops per cycle - Harmonic excitation

In this case, a harmonic excitation is accounted for, with a unit amplitude and a forcing frequency
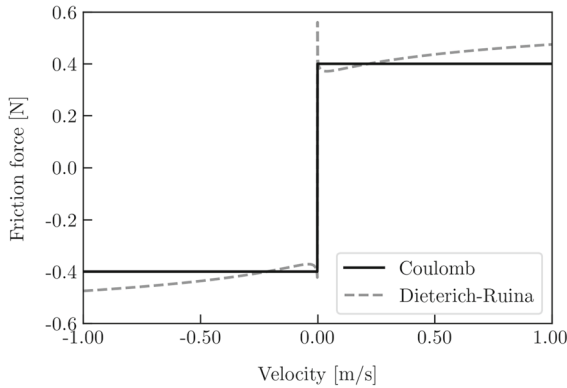
Fig. 2 Nonlinear friction force versus velocity for different friction laws

$\Omega = 0.3 \, \text{rad/s}$ to create measurements with two stops per cycle. Two friction laws, namely Coulomb (Case 1a) and steady-state Dieterich-Ruina (DR) [9,16,17] (Case 1b), are considered - both schematically illustrated in Fig. 2, where the nonlinear friction force is plotted against the velocity when considering arbitrary friction laws parameter values.

Within the Coulomb friction law, the friction term is explicitly dependent on the direction of movement, i.e. the sign of the velocity, when the mass is sliding. With its amplitude equal to the product of the friction coefficient μ between the two surfaces in contact and the normal force N, and denoting the friction force according to Coulomb law as F_C, it holds:

$$F_{\text{fr}}(t) = F_C(\dot{x}(t)) = \mu \, N \, \text{sgn}(\dot{x}(t)) \tag{38}$$

According to Eq. (29), the magnitudes of static and kinetic friction forces are considered equal. Moreover, in the case of sticking (when the velocity is zero), its value lies in the range of $[-1, 1]$, since the mass is in equilibrium, so the friction force is counterbalanced by the sum of the spring and external forces. For this friction model, a friction-to-forcing ratio $\mu \, N / F_0 = 0.5$ is chosen.

Denoting the friction force as F_{DR}, the steady-state formulation of DR [9] is:

$$F_{\text{fr}}(t) = F_{\text{DR}}(\dot{x}(t)) = \left[F_* + a \, \ln\left(\frac{|\dot{x}(t)| + \varepsilon}{V_*} \right) \right.$$
$$\left. + b \, \ln\left(c + \frac{V_*}{|\dot{x}(t)| + \varepsilon} \right) \right] \text{sgn}(\dot{x}(t)) \tag{39}$$

where F_* and V_* correspond to the steady-state friction force and sliding velocity reference values, a and

Table 3 Steady-state Dieterich-Ruina (DR) friction law properties

F_* [N]	a [–]	b [–]	c [–]	V_* [m/s]	ε [m/s]
0.5	0.07	0.09	0.022	0.003	10^{-6}

b are dimensionless model parameters, and parameter c which was originally proposed in [23], accounts for a residual strength at high sliding velocities. These parameters, of the steady-state DR law, are summarized in Table 3.

As indicated by [24], the $\boldsymbol{\theta}(\mathbf{x})$ dictionary should not include an abundance of candidate functions. The prior knowledge of the most suitable friction law is therefore used to guide their selection, as indicated in what follows.

Case 1a: Coulomb friction law
The employed feature dictionary is:

$$\boldsymbol{\theta}(x, y) = \begin{bmatrix} 1, \, x, \, y, \, x^2, \, x\,y, \, y^2 \end{bmatrix} \tag{40}$$

The hyperparameters of the analysis are summarized in Table 4.

The displacement and velocity fields identified by PhI-SINDy are plotted over time and illustrated in Fig. 3, where it is possible to observe a perfect agreement with the ground truth results.

The case where the event condition is not included - denoted in what follows as "PhI-SINDy without event condition" - is equivalent to applying the RK4-SINDy with the addition of the discrepancy bias. The comparison with PhI-SINDy is displayed in Fig. 4, where it is possible to observe the need to explicitly include the event condition to ensure accurate results.

Table 4 Hyperparameters for the synthetic cases (both SDOF and MDOF systems)

Quantity	Description	Value
M	Number of epochs	3×1000
lr	Learning rates	$1e-1, 1e-2, 1e-3$
λ	Cutoff threshold	$5e-2$
Δt	Time step	0.01 s
σ_{noise}	Measurement noise	10%

The number of epochs is expressed as 3×1000, because every 1000 epochs the learning rate is decreased, hence the three different lr values included

Fig. 3 Case 1a: Coulomb friction law Identified displacement and velocity fields
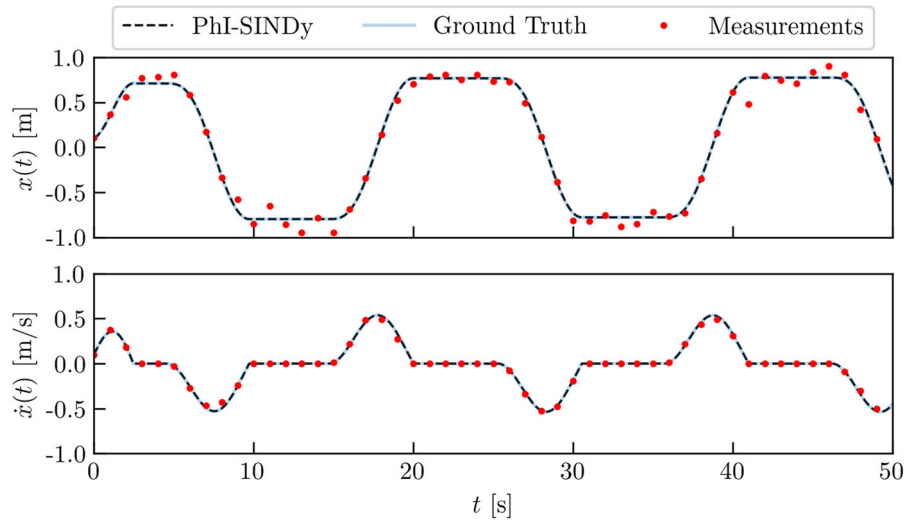
Fig. 4 Case 1a: Coulomb friction law Identified displacement and velocity fields, w/wo event condition
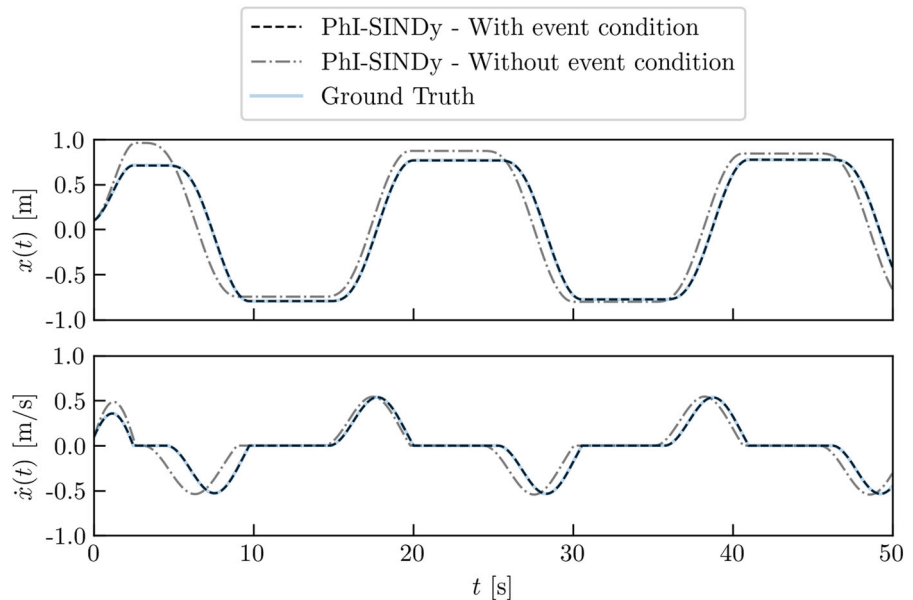
The governing equation identified both when including or not the event condition is the following:

Ground truth: $\dot{y} = -0.1\,y - x - 0.5\,\mathrm{sgn}(y) + \cos(0.3\,t)$

PhI-SINDy (with condition): $\dot{y} = -0.1\,y - x - 0.502\,\mathrm{sgn}(y) + \cos(0.3\,t)$
$$\tag{41}$$

PhI-SINDy (without condition): $\dot{y} = -0.1\,y - x - 0.354\,\mathrm{sgn}(y) + \cos(0.3\,t)$
$$\tag{42}$$

The identified EoM is parsimonious in both cases, even when the event condition to address stick–slip is not accounted for. This is attributed mainly to the appropriate terms that were included in the dictionary of functions. However, the identified coefficient of the friction term, as well as the plotted vector fields, when the event condition is included, highlight the superiority of the proposed framework when it comes to discontinuous nonlinearities.

In what follows, the comparison with PhI-SINDy without including the event condition will not be carried out, owing to its poor accuracy that is displayed in Fig. 4. The use of the term "PhI-SINDy" will imply that the sticking event condition is accounted for.

Case 1b: Dieterich-Ruina friction law

Assuming the dependency of the friction force to the sign of the velocity as part of the known physics, the candidate features include the possibility of choosing either or both Coulomb and DR coefficients:

$$\boldsymbol{\theta}(x, y) = \left[1, \ x, \ y, \ \ln\left(\frac{|y| + \varepsilon}{V_*}\right), \ \ln\left(c + \frac{V_*}{|y| + \varepsilon}\right)\right] \tag{43}$$

The identified displacement and velocity vector fields are presented in Fig. 5, showing also in this case an excellent agreement with the ground-truth results.

For presentation purposes, only the identified nonlinear friction term will be presented, compared with the ground truth.

Ground truth: $\left[0.5 + 0.07 \ln\left(\dfrac{|y| + 10^{-6}}{0.003}\right)\right.$

$\left. + 0.09 \ln\left(0.022 + \dfrac{0.003}{|y| + 10^{-6}}\right)\right] \text{sgn}(y)$

PhI-SINDy: $\left[0.493 + 0.049 \ln\left(\dfrac{|y| + 10^{-6}}{0.003}\right)\right.$

$\left. + 0.058 \ln\left(0.022 + \dfrac{0.003}{|y| + 10^{-6}}\right)\right] \text{sgn}(y) \tag{44}$

It is observed that also for this case PhI-SINDy manages to identify accurately the governing equation of the oscillator, with higher accuracy when it comes to the more dominant terms, such as F_*, and a slight deviation in the case of the smaller valued correction terms, a and b.

Comparison between Cases 1a and 1b

It is worth mentioning that PhI-SINDy can yield results of excellent agreement with the ground truth in both cases. A key difference between Cases 1a, and 1b, is the employed dictionary of functions, with second-order polynomial terms, and first-order polynomials together with two logarithmic terms, chosen in the case of Coulomb and DR friction law respectively, as shown in Eqs. (40) and (43). PhI-SINDy successfully picks the correct terms as part of the EoM and drops the redundant ones. It should be noted that the friction law parameters, a and b, employed in these cases, lie in a region of the parameter space where the two models lead to a similar but not identical response. To investigate the inverse problem where the responses are indistinguishable and the friction law is unknown, different parame-

ters a, b, and a dictionary including terms for both laws will be considered in Case 3.

4.1.1.2 Case 2: Four stops per cycle - Harmonic excitation

Using the same set of hyperparameters, a lower forcing frequency is accounted for, i.e. $\Omega = 0.15$ to increase the occurrence of stops per cycle to four.

Case 2a: Coulomb friction law

Using also the same dictionary of functions, presented in Eq. (40), the learned global response of the oscillator, which is in complete accordance with the ground truth, is displayed in Fig. 6.

The identified governing equation is:

Ground truth: $\quad \dot{y} = -0.1\, y - x - 0.5\, \text{sgn}(y) + \cos(0.15\, t)$
PhI-SINDy: $\quad \dot{y} = -0.1\, y - x - 0.5\, \text{sgn}(y) + \cos(0.15\, t)$
$$\tag{45}$$

Based both on the plotted time series as well as the identified acceleration field, it is obvious that the learned solution is identical to the ground truth, for a problem with more frequent sticking.

Case 2b: Dieterich-Ruina friction law

The same system is now examined considering the DR friction law as ground truth, and the feature dictionary of Eq. (43). The obtained displacement and velocity plots, which showcase the convergence of the identified solution with the ground truth, are shown in Fig. 7.

The identified EoM of the oscillator for a friction force generated according to the DR law is:

Ground truth: $\left[0.5 + 0.07 \ln\left(\dfrac{|y| + 10^{-6}}{0.003}\right)\right.$

$\left. + 0.09 \ln\left(0.022 + \dfrac{0.003}{|y| + 10^{-6}}\right)\right] \text{sgn}(y)$

PhI-SINDy: $\left[0.503 + 0.077 \ln\left(\dfrac{|y| + 10^{-6}}{0.003}\right)\right.$

$\left. + 0.099 \ln\left(0.022 + \dfrac{0.003}{|y| + 10^{-6}}\right)\right] \text{sgn}(y) \tag{46}$

These results highlight the ability of PhI-SINDy to address more complex friction laws, even when more excessive sticking occurs. Additionally, it can be observed that when more stops per cycle were present, a more accurate governing equation was identified (compared with Eq. (44)).

Fig. 5 Case 1b: Dieterich-Ruina friction law Identified displacement and velocity fields
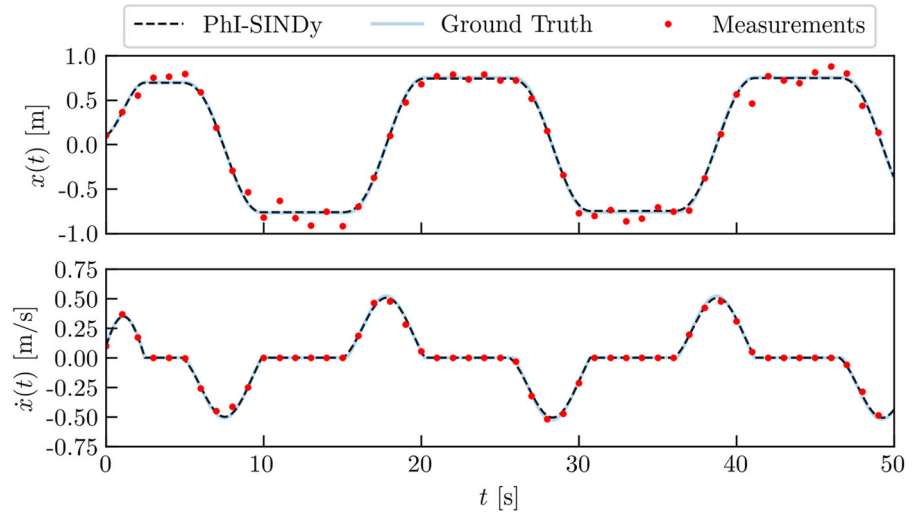
Fig. 6 Case 2a: Coulomb friction law Identified displacement and velocity fields
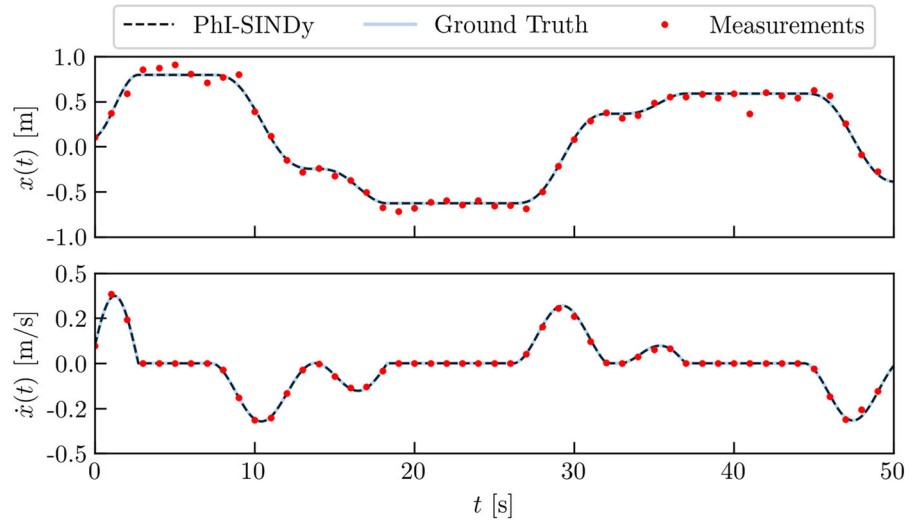
Fig. 7 Case 2b: Dieterich-Ruina friction law Identified displacement and velocity fields
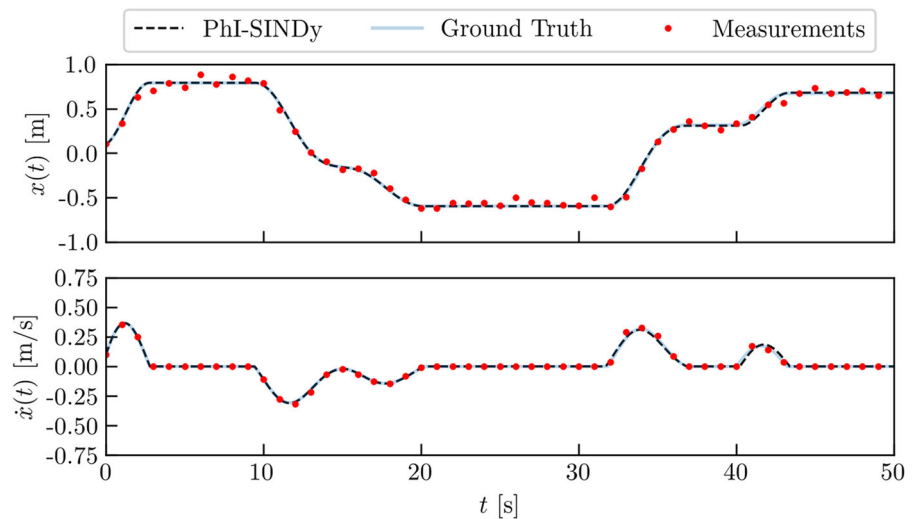
Table 5 Frition laws' properties that yield a similar response

F_0 [N]	Ω [rad/s]	$\mu\, N/F_0$ [–]	F_*/F_0 [–]	a [–]	b [–]	c [–]	V_* [m/s]	ε [m/s]
1.0	0.3	0.5	0.5	0.05	0.07	0.022	0.003	10^{-6}

Fig. 8 Mass displacement (**a**) and velocity (**b**) along forcing for two different friction laws

(a) Mass displacement vs forcing

(b) Mass velocity vs forcing
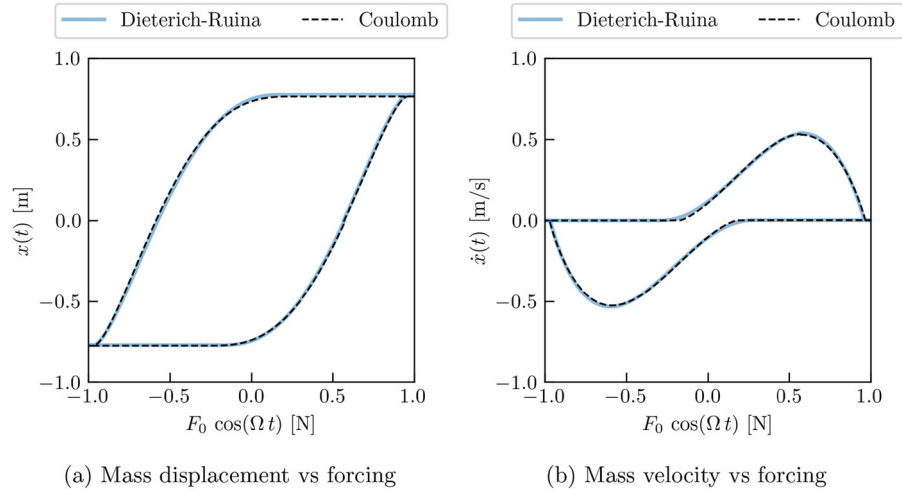
Comparison between Cases 2a and 2b

Similar conclusions, as for Cases 1a and 1b, can be drawn when comparing the two friction laws with more occurrences of sticking per cycle. The correct terms are kept in the identified EoM, while the coefficients referring to redundant terms are set to zero, leading ultimately to convergence with each ground truth.

4.1.1.3 Case 3: Inverse problem

An inverse problem in the identification of frictional systems is investigated. As elaborated in [9], there are regions in the (a) - $(b - a)$ parameter space, where the two friction models, i.e. Coulomb and DR, are almost indistinguishable under harmonic excitation of an SDOF. This similarity poses an additional obstacle to the identification problem and constitutes an interesting challenge for PhI-SINDy. Thus, a new set of parameters is considered, which are summarized in Table 5 along with the harmonic excitation parameters, that yield the forcing-displacement and forcing-velocity plots of Fig. 8. The dictionary of functions used is the general one reported in Eq. (43).

Initially, the noisy measurements are generated by considering the Coulomb friction law. The identified governing equation is:

Ground truth: $\dot{y} = -0.1\, y - x - 0.5\, \mathrm{sgn}(y) + \cos(0.3\, t)$
PhI-SINDy: $\dot{y} = -0.1\, y - x - 0.502\, \mathrm{sgn}(y) + \cos(0.3\, t)$
$$(47)$$

On the other hand, when the noisy measurements are generated using the steady-state DR friction law, the identified friction term is:

Ground truth: $\left[0.5 + 0.05\, \ln\!\left(\dfrac{|y| + 10^{-6}}{0.003} \right) \right.$
$$\left. + 0.07\, \ln\!\left(0.022 + \dfrac{0.003}{|y| + 10^{-6}} \right) \right] \mathrm{sgn}(y)$$

PhI-SINDy: $\left[0.507 + 0.04\, \ln\!\left(\dfrac{|y| + 10^{-6}}{0.003} \right) \right.$
$$\left. + 0.056\, \ln\!\left(0.022 + \dfrac{0.003}{|y| + 10^{-6}} \right) \right] \mathrm{sgn}(y)$$
$$(48)$$

It is possible to observe that PhI-SINDy is able to identify the correct friction law even for parameters that yield an almost identical system response.

Table 6 Jonswap spectrum parameters

H_s [m]	T_p [s]	ω_p [r/s]	$\sigma_p(\omega < \omega_p)$	$\sigma_p(\omega \geq \omega_p)$
10	0.5	$2\pi/T_p$	0.07	0.09

4.1.1.4 Case 4: Jonswap spectrum excitation

To check the robustness of the proposed methodology, a more complicated loading is also examined, in particular a random phase multi-sine whose amplitude is generated using the JONSWAP spectrum [18,25], and the parameters included in Table 6, which is illustrated in Fig. 9a:

$$S(\omega) = 320 \left(\frac{H_s}{T_p^2}\right)^2 \frac{1}{\omega^5}$$

$$\exp\left(-1.25\left(\frac{\omega_p}{\omega}\right)^4\right) 3.3^{\exp\left(-\frac{(\omega - \omega_p)^2}{2\,\sigma_p^2\,\omega_p^2}\right)} \quad (49)$$

In this forcing scenario, modified system parameters are used, to produce vector fields in a similar order of magnitude as the rest of the cases. In particular, a mass $m = 1$ kg, a viscous damping coefficient $c = 5$ N s m^{-1}, a stiffness $k = 500$ N m^{-1}, and a friction coefficient $\mu = 0.2$ are considered.

In such a case, the exact forcing time series is provided as part of the known physics, in a similar fashion, as with the monochromatic loading. Using the feature dictionary of Eq. (40), the identified displacement and velocity fields are indistinguishable from the ground truth, and are displayed in Fig. 10.

Denoting the external forcing as $F(t)$, the identified EoM is:

Ground truth: $\dot{y} = -5\,y - 64\,x - 0.2\,\mathrm{sgn}(y) + F(t)$

PhI-SINDy: $\dot{y} = -5\,y - 64\,x$
$$- 0.198\,\mathrm{sgn}(y) + F(t) \quad (50)$$

It is apparent that the identified governing equation converges to the ground truth, highlighting the high accuracy of the proposed identification scheme, even when the excitation, and subsequently the response, of the system is not an ideal harmonic input, as long as it is provided as part of the inductive bias. It should be noted, that in cases where a more complex excitation is present, even though it is explicitly provided to PhI-SINDy, an increase in the computational cost might be observed.

4.1.2 Multi degree of freedom (MDOF) system with one source of nonlinearity

Let us now consider a MDOF system, consisting of two masses m_1, m_2, that are connected with each other and with a fixed vertical wall with two springs and two dashpots, of stiffness k_1, k_2 and viscous damping coefficient c_1, c_2 respectively. The first mass is excited by an external force $F_1(t)$ and is able to slide in the horizontal direction through a roller, while the second mass is in contact with a fixed wall that generates the nonlinear friction force, $F_{\mathrm{fr},2}$. The configuration described above is illustrated in Fig. 11, and the EoMs of each mass are formulated as follows:

Fig. 9 Jonswap spectrum mass excitation
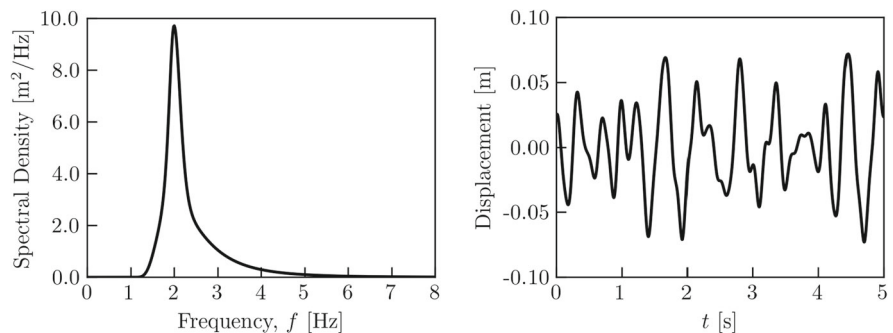
(a) JONSWAP spectrum [18]

(b) Random multi sine excitation generated using the JONSWAP spectrum

Fig. 10 Case 4: Jonswap spectrum excitation Identified displacement and velocity fields
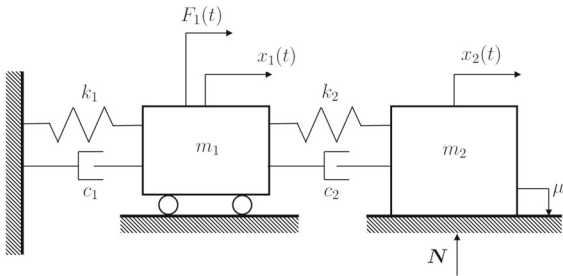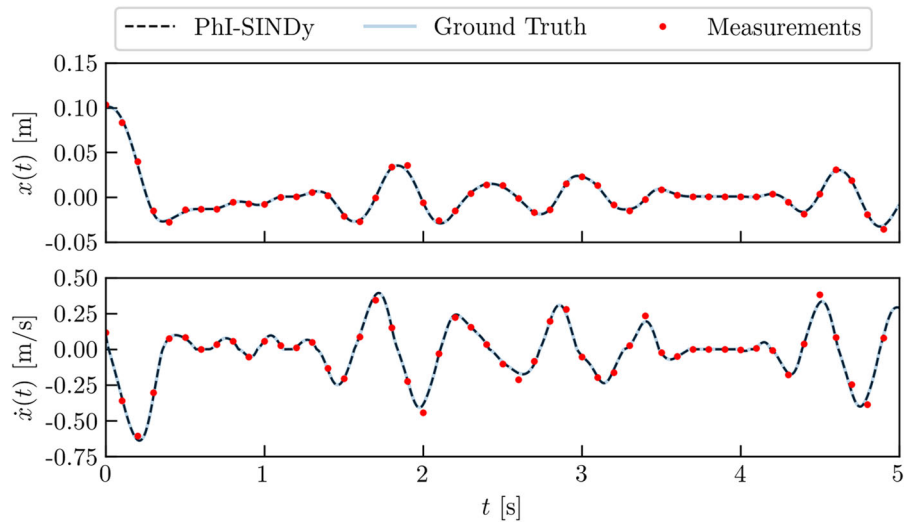
Fig. 11 MDOF system with one friction contact

$$m_1 \ddot{x}_1 + (c_1 + c_2) \dot{x}_1 - c_2 \dot{x}_2 + (k_1 + k_2) x_1$$
$$- k_2 x_2 = F_1(t) \tag{51}$$

$$m_2 \ddot{x}_2 + c_2 \dot{x}_2 - c_2 \dot{x}_1 + k_2 x_2 - k_2 x_1 + F_{\mathrm{fr},2}(t) = 0 \tag{52}$$

In a similar way as for the SDOF case, the EoMs are transformed in a state-space form, yielding the following coupled system of first-order differential equations:

$$\dot{x}_1 = y_1 \tag{53}$$

$$\dot{x}_2 = y_2 \tag{54}$$

$$\dot{y}_1 = \frac{1}{m_1} \Big[-(c_1 + c_2) y_1 + c_2 y_2 - (k_1 + k_2) x_1$$
$$+ k_2 x_2 + F_1(t) \Big] \tag{55}$$

$$\dot{y}_2 = \frac{1}{m_2} \Big[-c_2 y_2 + c_2 y_1 - k_2 x_2 + k_2 x_1 - F_{\mathrm{fr},2}(t) \Big] \tag{56}$$

Denoting the ratio of the two masses as $\bar{m} = m_2/m_1$, Eqs. (55)–(56) are rewritten as:

$$\dot{y}_1 = -(2 \zeta_1 \omega_1 + 2 \bar{m} \zeta_2 \omega_2) y_1$$
$$+ 2 \bar{m} \zeta_2 \omega_2 y_2 - (\omega_1 + \bar{m} \omega_2) x_1$$
$$+ \bar{m} \omega_2 x_2 + F_1(t) \tag{57}$$

$$\dot{y}_2 = -2 \zeta_2 \omega_2 y_2 + 2 \zeta_2 \omega_2 y_1 - \omega_2 x_2 + \omega_2 x_1$$
$$- F_{\mathrm{fr},2}(t) \tag{58}$$

where ω_1, ω_2 and ζ_1, ζ_2 are the natural frequency and the damping ratio.

A simple harmonic force is considered to be applied at mass m_1, while Coulomb's law describes the friction force generated due to the mass-wall contact. So, $F_1(t)$ and $F_{\mathrm{fr},2}$ are:

$$F_1(t) = 1.0 \cos(0.6\,t) \tag{59}$$

$$F_{\mathrm{fr},2}(t) = 0.3 \,\mathrm{sgn}(\dot{x}_2(t)) \tag{60}$$

The true displacement and velocity time series, $\mathbf{X}_{\mathrm{true}}$ for both masses are once more calculated using the explicit Runge–Kutta method of order 5(4) [22], and the system properties that are included in Table 7, incorporating an event condition to handle the transition between the sticking and sliding regimes. The noisy measurements X^* are generated according to Eq. (34), using the chosen noise level, σ_{noise}.

The sticking of m_2 is accounted for by considering the following event condition as a learning bias:

$$\begin{cases} \dot{x}_2(t) = 0 \\ |c_2 \dot{x}_1(t) + k_2 x_1(t) - k_2 x_2(t)| \leq |F_{\mathrm{fr},2}(t)| \end{cases} \tag{61}$$

As explained also for the SDOF oscillator, only the former of the two conditions is included in PhI-SINDy, owing to the noise sensitivity of the latter one.

Rewriting Eqs. (53), (54), (57), and (58) in a matrix format enables for a clearer distinction between the known, and unknown parts of the described system.

Ground truth: $\dot{y}_1 = -0.2\, y_1 + 0.1\, y_2$
$$- 2\, x_1 + x_2 + \cos(0.6\, t)$$
$$\dot{y}_2 = 0.1\, y_1 - 0.1\, y_2 + x_1 - x_2 - 0.5\, \mathrm{sgn}(y_2)$$

$$\mathbf{x} = \begin{bmatrix} x_1 \\ x_2 \\ y_1 \\ y_2 \end{bmatrix}$$

$$\begin{bmatrix} \dot{x}_1 \\ \dot{x}_2 \\ \dot{y}_1 \\ \dot{y}_2 \end{bmatrix} = \begin{bmatrix} 0 & 0 & 1 & 0 \\ 0 & 0 & 0 & 1 \\ -(\omega_1 + \bar{m}\,\omega_2)\,\bar{m}\,\omega_2 & -(2\,\zeta_1\,\omega_1 + 2\,\bar{m}\,\zeta_2\,\omega_2) & 2\,\bar{m}\,\zeta_2\,\omega_2 \\ \omega_2^2 & -\omega_2^2 & 2\,\zeta_2\,\omega_2 & -2\,\zeta_2\,\omega_2 \end{bmatrix} \cdot \begin{bmatrix} \dot{x}_1 \\ \dot{x}_2 \\ \dot{y}_1 \\ \dot{y}_2 \end{bmatrix} + \begin{bmatrix} 0 \\ 0 \\ \dfrac{F_1(t)}{m_1} \\ 0 \end{bmatrix} - \begin{bmatrix} 0 \\ 0 \\ 0 \\ \dfrac{F_{\mathrm{fr},2}(t)}{m_2} \end{bmatrix} \quad (62)$$

$$\Rightarrow \frac{\mathrm{d}}{\mathrm{d}t}\mathbf{x}(t) = \underbrace{\mathbf{g}(t,\,\mathbf{x}(t))}_{\substack{\text{known} \\ \text{physics}}} - \underbrace{\begin{bmatrix} 0 \\ 0 \\ 0 \\ \dfrac{F_{\mathrm{fr},2}(t)}{m_2} \end{bmatrix}}_{\substack{\text{part to be} \\ \text{identified}}} \quad (63)$$

$$\mathbf{g}(t,\,\mathbf{x}(t)) = \begin{bmatrix} 0 & 0 & 1 & 0 \\ 0 & 0 & 0 & 1 \\ -(\omega_1^2 + \bar{m}\,\omega_2^2)\,\bar{m}\,\omega_2^2 & -(2\,\zeta_1\,\omega_1 + 2\,\bar{m}\,\zeta_2\,\omega_2) & 2\,\bar{m}\,\zeta_2\,\omega_2 \\ \omega_2^2 & -\omega_2^2 & 2\,\zeta_2\,\omega_2 & -2\,\zeta_2\,\omega_2 \end{bmatrix} \cdot \mathbf{x}(t) + \begin{bmatrix} 0 \\ 0 \\ \dfrac{F_1(t)}{m_1} \\ 0 \end{bmatrix} \quad (64)$$

Also in this case, the system parameters in the known physics part are assumed to be deterministic.

4.1.2.1 Case 5: MDOF with one nonlinearity (Coulomb)

For this system a more specific dictionary of functions is needed, including only first-order polynomials:

$$\boldsymbol{\theta}(x_1, y_1, x_2, y_2) = [1,\ x_1,\ y_1,\ x_2,\ y_2] \quad (65)$$

The identified displacement and velocity vector fields for both masses, using the same hyperparameters presented in Table 4, are identical to the ones corresponding to the ground truth and are illustrated in Fig. 12.

Also for this case, a comparison between PhI-SINDy when an event condition is included and when not is investigated and plotted in Fig. 13. The corresponding identified governing equations are:

Table 7 MDOF system general properties

Quantity	Description	Value	Units
m_1	Mass	1	kg
m_2	Mass	1	kg
c_1	Viscous damping coefficient	0.1	Ns/m
c_2	Viscous damping coefficient	0.1	Ns/m
k_1	Stiffness	1	N/m
k_2	Stiffness	1	N/m
$x_1(0)$	Initial displacement of m_1 (at $t = 0$)	0.0	m
$x_2(0)$	Initial displacement of m_2 (at $t = 0$)	0.0	m
$\dot{x}_1(0)$	Initial velocity of m_1 (at $t = 0$)	0.0	m/s
$\dot{x}_2(0)$	Initial velocity of m_2 (at $t = 0$)	0.0	m/s

Fig. 12 Case 5: MDOF with one nonlinearity (Coulomb) Identified displacement and velocity fields
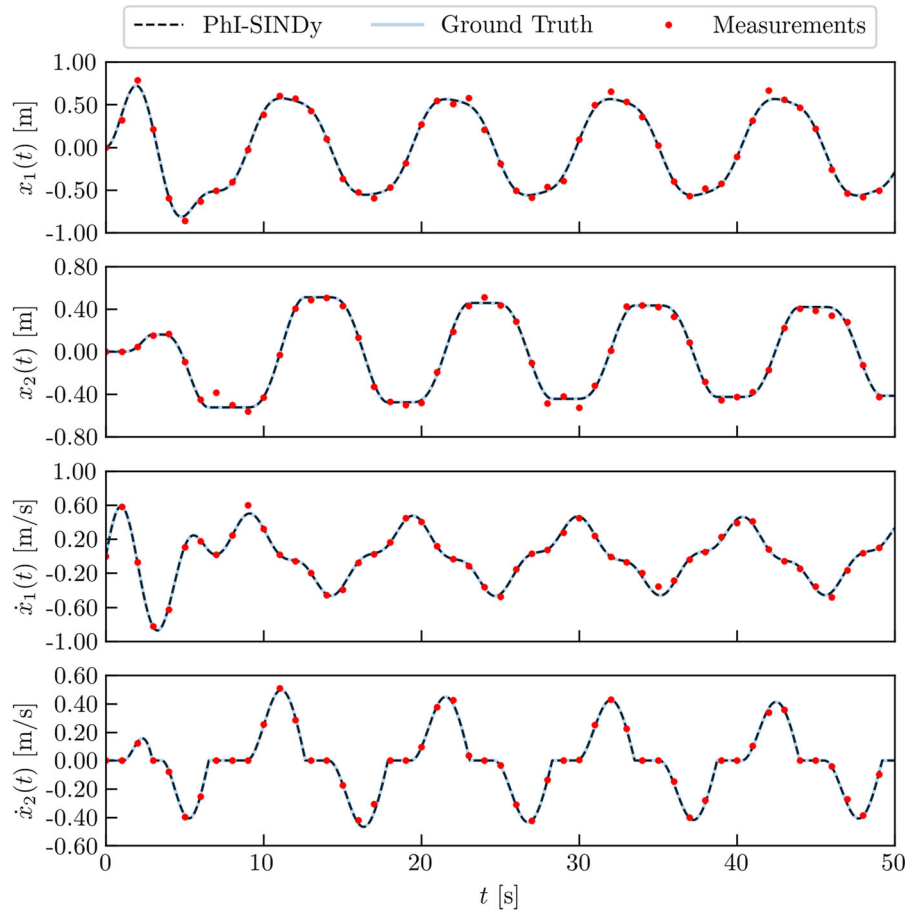
PhI-SINDy (with condition):

$$\dot{y}_1 = -0.2\, y_1 + 0.1\, y_2 - 2\, x_1 + x_2 + \cos(0.6\, t)$$

$$\dot{y}_2 = 0.1\, y_1 - 0.1\, y_2 + x_1 - x_2 - 0.5\, \mathrm{sgn}(y_2)$$

PhI-SINDy (without condition:

$$\dot{y}_1 = -0.2\, y_1 + 0.1\, y_2 - 2\, x_1 + x_2 + \cos(0.6\, t)$$

$$\dot{y}_2 = 0.1\, y_1 - 0.1\, y_2 + x_1 - x_2 - 0.389\, \mathrm{sgn}(y_2)$$

$$(66)$$

Both the displacement and velocity fields and the identified EoMs, confirm that including a sticking event condition leads to a more accurate identification.

4.1.3 Multi degree of freedom (MDOF) system with two sources of nonlinearity

To highlight the potential of the proposed framework, a system with multiple sources of discontinuous nonlinearity is accounted for. In particular, the same MDOF system is considered, with both masses being in contact with an immovable wall, thus each being subjected to an independent nonlinear friction force, as displayed in Fig. 14.

The system properties are the same as before, with the only difference being the additional friction force. Thus, Eqs. (57) and (58), are transformed into:

$$\dot{y}_1 = -(2\,\zeta_1\,\omega_1 + 2\,\bar{m}\,\zeta_2\,\omega_2)\, y_1 + 2\,\bar{m}\,\zeta_2\,\omega_2\, y_2$$
$$- (\omega_1 + \bar{m}\,\omega_2)\, x_1 + \bar{m}\,\omega_2\, x_2 - F_{\mathrm{fr},1}(t) + F_1(t) \tag{67}$$

$$\dot{y}_2 = -2\,\zeta_2\,\omega_2\, y_2 + 2\,\zeta_2\,\omega_2\, y_1 - \omega_2\, x_2 + \omega_2\, x_1$$
$$- F_{\mathrm{fr},2}(t) \tag{68}$$

Therefore, the vector containing known physics, $\mathbf{g}(\mathbf{x}(t))$ stays as is, and only the part to be identified changes into:

Fig. 13 Case 5: MDOF with one nonlinearity (Coulomb) Identified displacement and velocity fields, w/wo event condition)
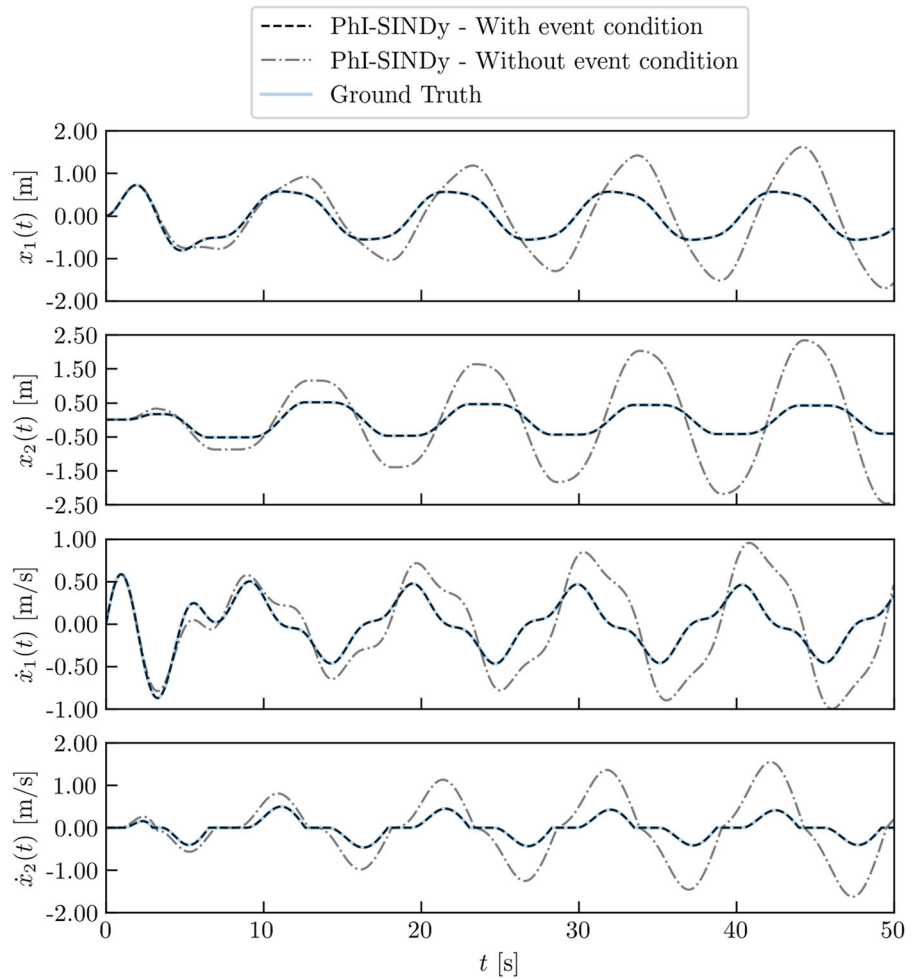
$$
\begin{bmatrix}
0 \\
0 \\
\dfrac{F_{\mathrm{fr},1}(t)}{m_1} \\
\dfrac{F_{\mathrm{fr},2}(t)}{m_2}
\end{bmatrix}
\tag{69}
$$

Concerning the stick–slip phase of the system, a different event condition for each mass is included in the learning process:

Mass m_1
$$
\begin{cases}
\dot{x}_1(t) = 0 \\
|F_1(t) + c_2\,\dot{x}_2(t) + k_2\,x_2(t) \\
\quad -(k_1 + k_2)\,x_1(t)| \le |F_{\mathrm{fr},1}(t)|
\end{cases}
\tag{70}
$$

Mass m_2
$$
\begin{cases}
\dot{x}_2(t) = 0 \\
|c_2\,\dot{x}_1(t) + k_2\,x_1(t) - k_2\,x_2(t)| \le |F_{\mathrm{fr},2}(t)|
\end{cases}
\tag{71}
$$

It should be noted that due to the presence of noise, only the zero-velocity condition of both masses are utilized as PhI-SINDy's physics constraint.

4.1.3.1 Case 6: MDOF with two nonlinearities (both Coulomb)

Firstly, both friction forces are assumed to be described by Coulomb's law, and expressed as:

$$
F_{\mathrm{fr},1}(t) = 0.5\,\mathrm{sgn}(\dot{x}_1(t))
\tag{72}
$$
$$
F_{\mathrm{fr},2}(t) = 0.3\,\mathrm{sgn}(\dot{x}_2(t))
\tag{73}
$$

Using the same feature dictionary as in Eq. (65), and the same hyperparameters presented in Table 4, the identified displacement and velocity fields are illustrated in Fig. 15.

It is apparent that the identified vector fields are identical to the ground truth. Furthermore, the identified EoM for each of the masses, along with the ground
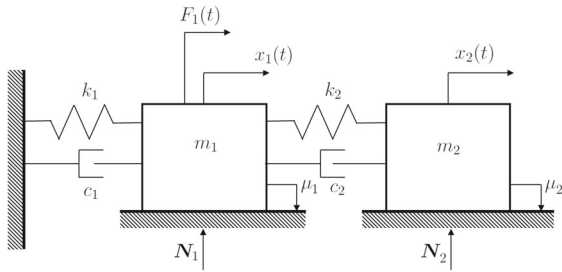
Fig. 14 MDOF system with two friction contacts

truth formulation are:

Ground truth: $\dot{y}_1 = -0.2\ y_1 + 0.1\ y_2 - 2\ x_1$
$+ x_2 - 0.5\mathrm{sgn}(y_1) + \cos(0.6\ t)$
$\dot{y}_2 = 0.1\ y_1 - 0.1\ y_2 + x_1 - x_2 - 0.3\ \mathrm{sgn}(y_2)$
PhI-SINDy: $\dot{y}_1 = -0.2\ y_1 + 0.1\ y_2 - 2\ x_1$
$+ x_2 - 0.501\mathrm{sgn}(y_1) + \cos(0.6\ t)$

$$\dot{y}_2 = 0.1\ y_1 - 0.1\ y_2 + x_1 - x_2 - 0.3\ \mathrm{sgn}(y_2) \quad (74)$$

It is observed that PhI-SINDy is capable to produce results that converge to the ground truth. Redundant terms are not included in the final solution, and the identified friction coefficients approach their true values.

4.1.3.2 Case 7: MDOF with two nonlinearities (Coulomb and Dieterich-Ruina) Let us now consider, the same MDOF system, but different friction laws to describe the discontinuous forces generated by the contact of the masses with the immovable walls. To elaborate, the two friction forces are expressed as:

$$F_{\mathrm{fr},1}(t) = 0.3\ \mathrm{sgn}(y_1(t)) \quad (75)$$

$$F_{\mathrm{fr},2}(t) = \left[0.3 + 0.07\ \ln\left(\frac{|y_2| + 10^{-6}}{0.003}\right)\right.$$

Fig. 15 Case 6: MDOF with two nonlinearities (both Coulomb) Identified displacement and velocity fields

$$+0.09 \ln\left(0.022 + \frac{0.003}{|y_2| + 10^{-6}}\right)\Bigg] \text{sgn}(y_2) \tag{76}$$

The employed dictionary of candidate function for this case is:

$$\boldsymbol{\theta}(\mathbf{x}) = \begin{bmatrix} 1, x_1, x_2, y_1, y_2, \\ \ln\left(\dfrac{|y_1| + \varepsilon}{V_*}\right), \\ \ln\left(\dfrac{|y_2| + \varepsilon}{V_*}\right), \\ \ln\left(c + \dfrac{V_*}{|y_1| + \varepsilon}\right), \ln\left(c + \dfrac{V_*}{|y_2| + \varepsilon}\right) \end{bmatrix} \tag{77}$$

The identified displacement and velocity vector fields for each of the masses are plotted in Fig. 16.

It is observed that the solution yielded by PhI-SINDy is less accurate compared to the ground truth, which is further highlighted by the identified friction forces where one of the logarithm terms is dropped in favor of polynomial terms:

Ground truth:

$$F_{\text{fr},1} = 0.3\text{sgn}(y_1)$$

$$F_{\text{fr},2} = V\Bigg[0.3 + 0.07 \ln\left(\frac{|y_2| + 10^{-6}}{0.003}\right)$$

$$+0.09 \ln\left(0.022 + \frac{0.003}{|y_2| + 10^{-6}}\right)\Bigg] \text{sgn}(y_2)$$

PhI-SINDy:

$$F_{\text{fr},1} = 0.302\text{sgn}(y_1)$$

$$F_{\text{fr},2} = \Big[0.294 + 0.22\,x_1 - 0.145\,x_2 - 0.131\,y_1$$

$$- 0.11\,y_2$$

$$-0.034 \ln\left(0.022 + \frac{0.003}{|y_2| + 10^{-6}}\right)\Bigg] \text{sgn}(y_2) \tag{78}$$

In this case, expert knowledge can be further supplied, since the presence of one of the logarithm terms in the second friction force identified is pointing toward a DR friction law, rather than a Coulomb friction one. This can be achieved by specifying a restricted number of candidate functions for the second friction force identification, and/or by setting a different cutoff threshold parameter. For the case at hand, a more specific set of candidate functions is chosen, to highlight the

importance of supplying further domain knowledge in the identification process. In particular, the first-order polynomial terms are removed, so the feature dictionary used is:

$$\boldsymbol{\theta}(x_1, x_2, y_1, y_2) = \begin{bmatrix} 1, \ln\left(\dfrac{|y_1| + \varepsilon}{V_*}\right), \\ \ln\left(c + \dfrac{V_*}{|y_1| + \varepsilon}\right), \\ \ln\left(\dfrac{|y_2| + \varepsilon}{V_*}\right), \\ \ln\left(c + \dfrac{V_*}{|y_2| + \varepsilon}\right) \end{bmatrix} \tag{79}$$

This additional bias improves significantly the accuracy of PhI-SINDy, which yields the following EoMs, and the identified vector fields displayed in Fig. 17.

Ground truth:

$$F_{\text{fr},1} = 0.3\text{sgn}(y_1)$$

$$F_{\text{fr},2} = \Bigg[0.3 + 0.07 \ln\left(\frac{|y_2| + 10^{-6}}{0.003}\right)$$

$$\ln\left(0.022 + \frac{0.003}{|y_2| + 10^{-6}}\right)\Bigg] \text{sgn}(y_2)$$

PhI-SINDy:

$$F_{\text{fr},1} = 0.3\text{sgn}(y_1)$$

$$F_{\text{fr},2} = \Bigg[0.286 + 0.062 \ln\left(\frac{|y_2| + 10^{-6}}{0.003}\right)$$

$$74 \ln\left(0.022 + \frac{0.003}{|y_2| + 10^{-6}}\right)\Bigg] \text{sgn}(y_2) \tag{80}$$

It is apparent that both in terms of the governing equations' functional form and the plotted displacement and velocity fields, the identified solution converges to the ground truth. To elaborate, given additional expert knowledge PhI-SINDy yields a parsimonious solution with no redundant terms, and the coefficients of the included terms approach their true values.

4.2 Experimental cases

Let us consider the laboratory configuration [21] of an SDOF oscillator illustrated in Fig. 18. This setup constitutes the experimental counterpart of the SDOF

Fig. 16 Case 7: MDOF with two nonlinearities (Coulomb and Dieterich-Ruina) Identified displacement and velocity fields
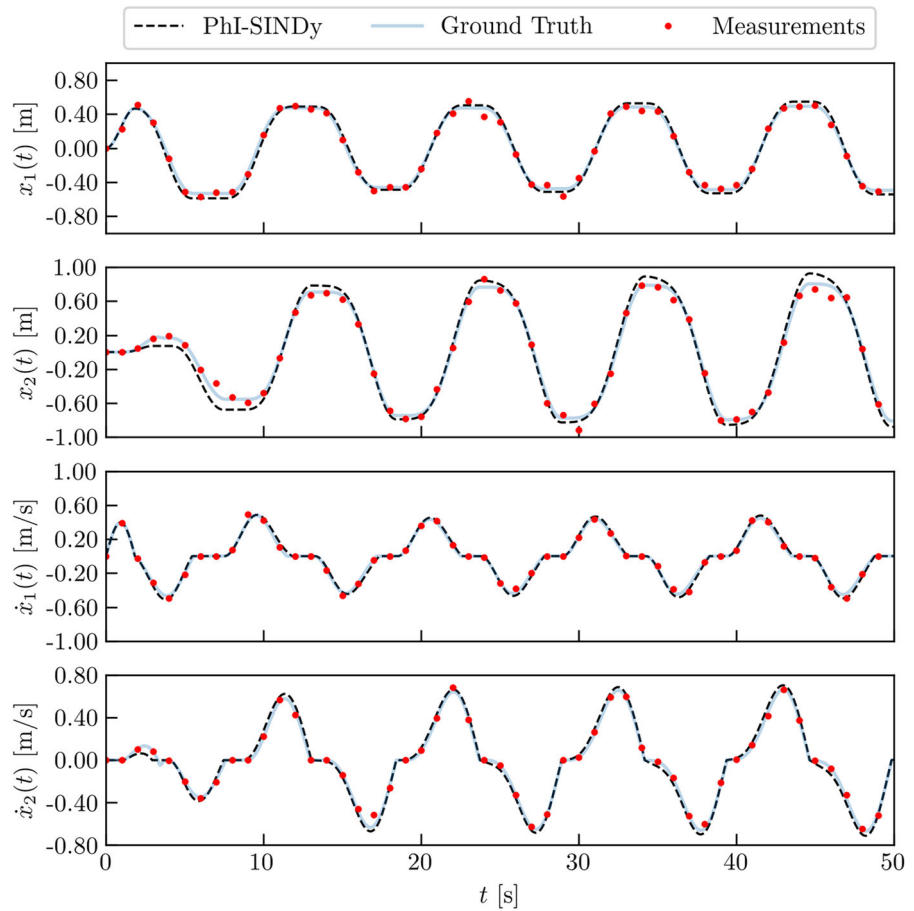
system introduced in Sect. 4.1.1, meaning that the presented EoM, friction laws, and the distinction between sticking and sliding are still valid for this case.

It is essential for such a case to provide the correct physics to the framework. Contrary to the synthetic cases, where the ground truth values can be tuned or modified, the system properties in a real-life setup can only be estimated. In case the wrong physics (or none at all) is provided, this discrepancy with the true values will be encapsulated in the sought nonlinear terms. Thus, instead of an analytical form of the forcing, which is not available, the base excitation, $u(t)$, is used. Both the forcing data and the response to it, $x(t)$, are measured with laser displacement sensors as indicated in Fig. 18. For the derivation of the corresponding velocity time series, $\dot{x}(t)$ and $\dot{u}(t)$, a smooth automatic differentiation is utilized, and Eq. (25) is transformed into:

$$
\begin{aligned}
\ddot{x}(t) = &-2\,\zeta\,\omega_n\,\dot{x}(t) - \omega_n^2\,x(t) - F_{\mathrm{fr}}(t) \\
&+2\,\zeta\,\omega_n\,\dot{u}(t) + \omega_n^2\,u(t)
\end{aligned} \tag{81}
$$

Table 8 Experimental setup properties

Quantity	Description	Value	Units
m	Mass	3.080	kg
c	Viscous damping coefficient	0.203	Ns/m
k	Stiffness	1190	N/m
μ	Friction coefficient	0.278	[–]
M	Mass of sliding disc	0.097	kg
$N = M\,g$	Normal force	0.950	N

The identification of the governing equation of the system at hand is first attempted by assuming Coulomb's friction law. The properties of the system are measured or estimated and they are listed in Table 8. By allowing the system to vibrate freely with and without the contact on top and postprocessing its fading oscillation, the harder-to-calculate damping and friction coefficients, c and μ were estimated.

Fig. 17 Case 7: MDOF with two nonlinearities (Coulomb and Dieterich-Ruina) Identified displacement and velocity fields including user knowledge
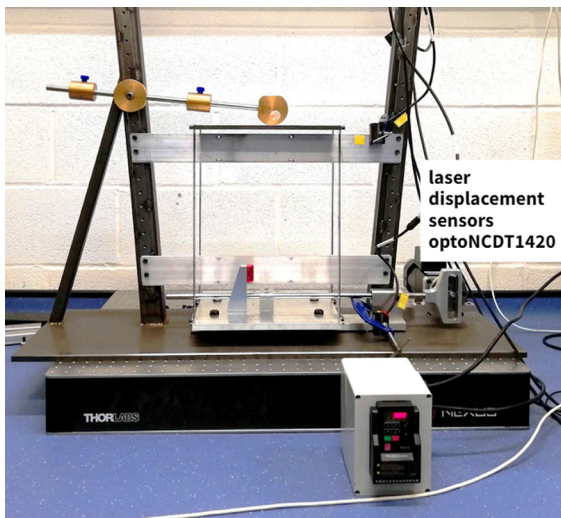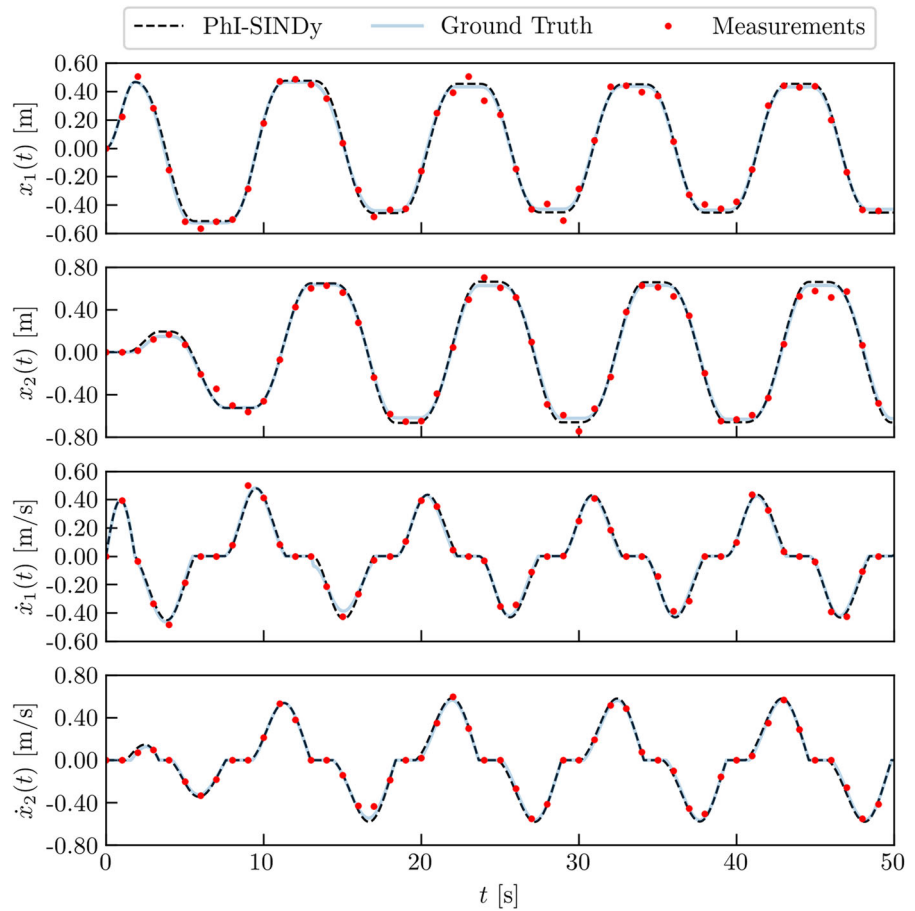
Fig. 18 Experimental setup of an SDOF with friction contact obtained with a counter-weight system mounted on a fixed wall subject to a harmonic-based excitation [21]

Substituting these values in Eq. (81), the ground truth for this experimental case study is:

$$
\begin{aligned}
\ddot{x}(t) = &-0.0658\,\dot{x}(t) - 386.36\,x(t) \\
&-0.0856\,\mathrm{sgn}(\dot{x}(t)) \\
&+0.0658\,\dot{u}(t) + 386.36\,u(t)
\end{aligned}
\tag{82}
$$

Lastly, regarding the discrepancy bias, similar to the synthetic SDOF case, it holds:

$$
\mathbf{x}(t) = \begin{bmatrix} x(t) \\ y(t) \end{bmatrix} = \begin{bmatrix} x(t) \\ \dot{x}(t) \end{bmatrix} \quad , \quad \mathbf{u}(t) = \begin{bmatrix} u(t) \\ \dot{u}(t) \end{bmatrix} \Rightarrow \frac{\mathrm{d}}{\mathrm{d}t}\mathbf{x}(t)
\tag{83}
$$

$$
= \underbrace{\begin{bmatrix} 0 & 1 \\ -\omega_n^2 & -2\,\zeta\,\omega_n \end{bmatrix} \cdot \mathbf{x}(t) + \begin{bmatrix} 0 & 0 \\ -\omega_n^2 & -2\,\zeta\,\omega_n \end{bmatrix} \cdot \mathbf{u}(t)}_{\text{known physics, } \mathbf{g}(t,\,\mathbf{x}(t))} - \underbrace{\begin{bmatrix} 0 \\ \dfrac{F_{\mathrm{fr}}(t)}{m} \end{bmatrix}}_{\substack{\text{part to be} \\ \text{identified}}}
\tag{84}
$$

Different hyperparameters are employed in this case, which are summarized in Table 9.

Table 9 Hyperparameters for the experimental case

Quantity	Description	Value
M	Number of epochs	3×2000
lr	Learning rates	$1e-1, 1e-2, 1e-3$
λ	Cutoff threshold	$1e-2$
Δt	Time step	$5e-4$ s

4.2.1 Case 8: Experiment with a friction contact - Continuous motion

To elaborate on the importance of including the exact measurements of the base excitation, three different cases are examined, for the continuous motion of the oscillator, namely (a) including the measured base displacement, (b) omitting any system knowledge about forcing (data-driven approach), and (c) assuming a perfect harmonic excitation. For all three cases, it is again assumed that the friction is dependent on the direction of movement. Apart from first-order polynomial terms, multiplied by $\text{sgn}(y(t))$, harmonic terms are also considered candidate features. Five different frequencies, Ω_i, are accounted for, surrounding the excitation one, which is determined through the Fast Fourier Transform. Thus, the dictionary of functions is:

$$\boldsymbol{\theta}(x, y) = \begin{bmatrix} \text{sgn}(y), \ x\,\text{sgn}(y(t)), \ y\,\text{sgn}(y(t)), \\ \cos(\Omega_i\,t) \end{bmatrix} \quad (85)$$

The identified governing equations for each of the three approaches are:

Truth: $\quad \dot{y} = -0.0658\,y - 386.36\,x - 0.0856\,\text{sgn}(y)$
$\qquad\qquad + 0.0658\,\dot{u} + 386.36\,u$

(a): $\quad \dot{y} = -0.0658\,y - 386.36\,x - 0.0876\,\text{sgn}(y)$
$\qquad\qquad + 0.0658\,\dot{u} + 386.36\,u \quad (86)$

(b): $\quad \dot{y} = -66.88\,y - 305.34\,x - 0.120\,\text{sgn}(y)$
$\qquad\qquad + 3.419\,\cos(13.5\,t) \quad (87)$

(c): $\quad \dot{y} = -12.10\,y - 206.79\,x - 0.102\,\text{sgn}(y)$
$\qquad\qquad + 0.722\,\cos(13.5\,t) \quad (88)$

All three variations yield results that converge to the ground truth response when plotting the displacement and velocity fields. For presentation purposes, since it would be visually confusing to plot three overlapping curves, only (b) is presented along the measurements and the ground truth in Fig. 20.

It should be noted that for all three approaches, the terms $-0.0658\,y - 386.36\,x$ are considered known (inductive bias), and in case (a) also the terms $0.0658\,\dot{u} + 386.36\,u$. To elaborate, the inclusion of the exact excitation led to dropping any linear x and y terms, while in (b) and (c), apart from the additional harmonic terms that represent the forcing, there are also considerable residual stiffness and damping terms. Even though the data is fitted efficiently, only including the measured base motion resulted also in a generalizable governing equation.

4.2.2 Case 9a: Experiment - Two stops per cycle - Coulomb

Using the same laboratory setup but with a lower base excitation frequency, the measured system's response contains stick–slip phenomena with two stops per cycle. Regarding the employed dictionary of functions, second-order polynomial features are considered, as in Eq. (40), and the exact forcing measurements are included in the scheme, based on the superior findings that were presented above. Its performance is displayed in Fig. 20.
The identified EoM is:

Ground Truth: $\quad \dot{y} = -0.0658\,y - 386.36\,x$
$\qquad\qquad\quad - 0.0856\,\text{sgn}(y) + 0.0658\,\dot{u}$
$\qquad\qquad\quad + 386.36\,u$

PhI-SINDy: $\quad \dot{y} = -0.0658\,y - 386.36\,x$
$\qquad\qquad\quad - 0.082\,\text{sgn}(y) + 0.0658\,\dot{u}$
$\qquad\qquad\quad + 386.36\,u \quad (89)$

The solution generated by PhI-SINDy converges to the ground truth, both in terms of plots and the underlying EoM, also for a real-life oscillator with nonsmooth and nonlinear behavior.

4.2.3 Case 9b: Experiment - Two stops per cycle - Dieterich-Ruina

For the same set of excitation and response measurements, the more generic dictionary of candidate functions is considered (Eq. (43)), yielding the results presented in the plot of Fig. 21.
The identified nonlinear friction force is:

PhI-SINDy: $\quad \left[0.083 + 0.100\,\ln\!\left(\dfrac{|y| + \varepsilon}{V_*} \right) \right.$

Fig. 19 Case 8: Experiment with a friction contact - Continuous motion Identified displacement and velocity fields
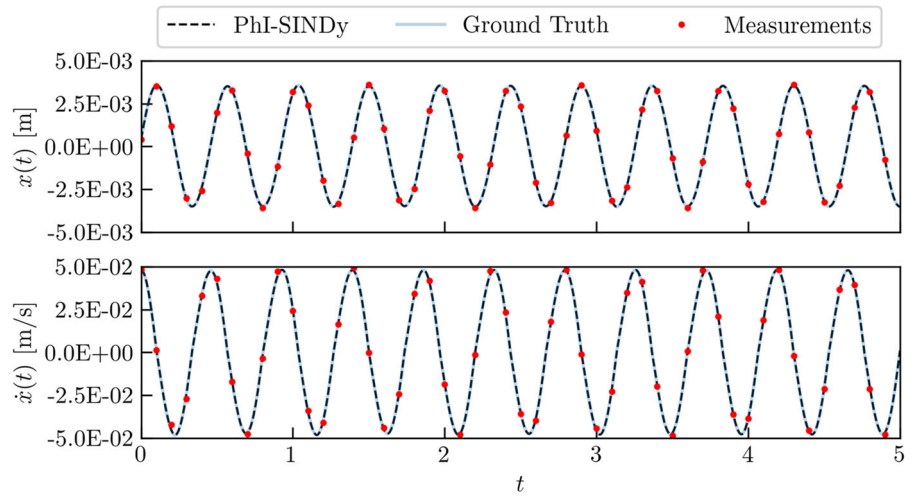
Fig. 20 Case 9a: Experiment - Two stops per cycle - Coulomb Identified displacement and velocity fields
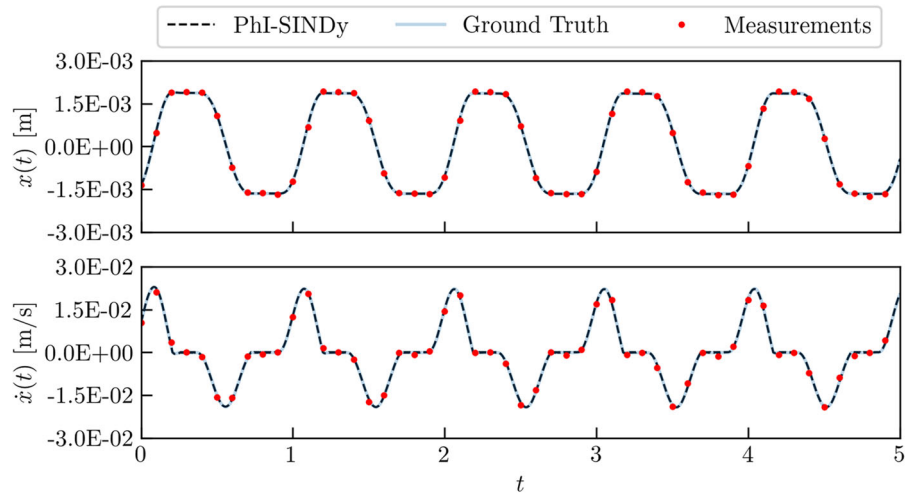
Fig. 21 Case 9b: Experiment - Two stops per cycle - Dieterich-Ruina Identified displacement and velocity fields
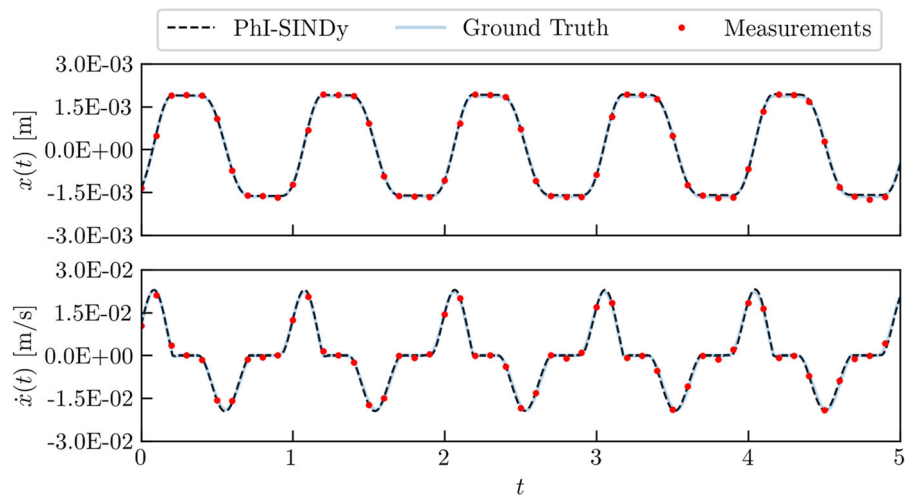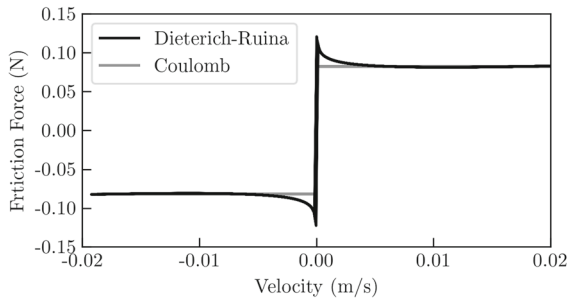
Fig. 22 Case 9a and 9b: Identified nonlinear force over velocity

$$+0.108\,\ln\!\left(0.022+\frac{V_*}{|y|+\varepsilon}\right)\right]\,\mathrm{sgn}(y) \qquad (90)$$

Even though there is no estimation available for the correction terms a and b of the employed friction law, their identified values yield vector fields that fit accurately the measurement. In the case of the F_* term, its identified value, 0.083, converges to the estimated friction term coefficient.

Comparison between Cases 9a and 9b

It should be mentioned that even though in both cases PhI-SINDy fits the measured data, when both Coulomb and DR candidate features are considered (Case 9b), the logarithmic terms are kept in the final solution, hinting that the DR friction law is the most appropriate for the dataset at hand. The friction force in both cases is plotted over the velocity in Fig. 22, to illustrate the identified friction laws.

4.2.4 Case 10: Experiment - Four stops per cycle - Coulomb

For the last case, let us consider more occurrences of sticking per cycle, namely four. The candidate features of Eq. (40) are accounted for, yielding the results illustrated in Fig. 23, which coincide with the ground truth, and the following governing equation:

$$\text{Ground Truth:} \quad \dot{y} = -0.0658\,y - 386.36\,x$$
$$- 0.0856\,\mathrm{sgn}(y) + 0.0658\,\dot{u}$$
$$+ 386.36\,u$$
$$\text{PhI-SINDy:} \quad \dot{y} = -0.0658\,y - 386.36\,x$$
$$- 0.0855\,\mathrm{sgn}(y) + 0.0658\,\dot{u}$$
$$+ 386.36\,u \qquad (91)$$

It is observed that PhI-SINDy identifies accurately the EoM and the displacement and velocity fields, also for the case where more sticking occurrences are present.

5 Recommendations

Based on a large number of case studies investigated, the following recommendations on the use of PhI-SINDy can be drawn:

1. **Data pre-processing step**

   - There is a need to perform a quality check on the noisy measurements at hand. An important issue is the selection of an appropriate sampling frequency able to capture in sufficient detail the relevant frequency content of the phenomena being investigated.
   Another issue is the involuntary presence of confounding sources (e.g. environmental conditions, unsuitable operating conditions, inappropriate setup of the monitoring system).

   - It has been observed that providing measurements that include both transient and steady-state responses led to increased accuracy in the sparse identification for some cases. However, it is not possible to suggest a rule-of-thumb on the length of transient and steady-state portions, since this is heavily case-dependent.

   - In the examined experimental cases only the displacement measurements were available, implying that velocity needs to be calculated from noisy displacement data, which is not a trivial task. It is advised, if possible to use directly velocity measurements. Alternatively, if only displacement measurements are available, a differentiation step is necessary. The derived velocity measurements need to be checked, as the selection of the most suitable differentiation algorithm relies heavily on the dataset at hand, and especially on the dataset noise level. For instance, in the experimental cases of the current paper, the differentiation step is performed using the spectral method.

2. **Selecting learning architecture step**

   - A preliminary run of RK4-SINDy with a sufficiently broad dictionary of functions is rec-

ommended, especially in cases where there are doubts regarding the known physics. In this way, the important features are determined, and the function space is reduced, improving the accuracy of PhI-SINDy.

- In the presence of discontinuous nonlinear terms the identified governing equation might not converge to the ground truth, owing to the lack of an appropriate constraint being specified. Whenever known, physics-based constraints should be specified to reduce the space of possible sparse solutions.

3. **Validation step**

- Having chosen the learning architecture, multiple datasets of the same dynamical system, that do not refer to the same excitation and response, should be examined. For instance, for problems with friction, one dataset could refer to an excitation leading to continuous motion, and another to stick–slip. These runs would act as a cross-validation step on the identified sparse solution.

Finally, it is worth stressing again three key points that require further attention: (i) in its current setup, PhI-SINDy identifies the unknown terms of the governing equation without quantifying any remaining uncertainty; (ii) including one or more wrong physics biases would result in exploring a wrong region of the solution space, hindering the accuracy of the sparse solution; (iii) the selection of the cut-off value is still manually tuned, and should be automated.

6 Conclusions

An extension to RK4-SINDy has been proposed to efficiently identify the nonsmooth response of dynamical systems when discontinuous nonlinearities are present. The proposed method, namely Physics Encoded. Sparse Identification of Nonlinear Dynamics (PhI-SINDy) requires: (i) a single set of input and output measurements of sufficient length, e.g. the excitation and the response of a system to it (ideally including both transient and steady-state responses); (ii) a selection of candidate functions that can possibly describe the sought EoM (inductive bias); (iii) part of the known physics, which shifts the focus on the identification of the more cumbersome discontinuous terms (discrepancy bias); (iv) an event condition that acts as a physical constraint and addresses the discontinuous behavior of the underlying functions (inductive bias); (v) the modification of the learning algorithm, and especially the fourth-order Runge–Kutta integration scheme, to incorporate the provided known physics and physical constraints (learning bias).

PhI-SINDy was applied to a variety of systems, using both synthetic and experimental data. An SDOF oscillator with Coulomb friction, under harmonic excitation, was considered at first, moving on to more elaborate friction laws, more complicated forcing, and finally to an MDOF with multiple sources of nonlinearity.

PhI-SINDy achieved an improved identification of the underlying governing equations based on noisy input and output measurements compared with methods that do not utilize domain knowledge. A signif-

Fig. 23 Case 10: Experiment - Four stops per cycle - Coulomb Identified displacement and velocity fields
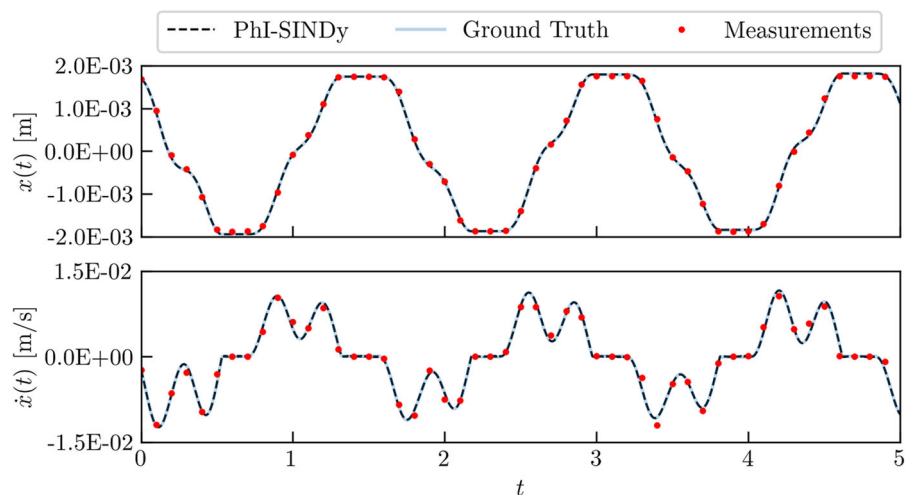
icant achievement was the system identification in a discontinuous regime, i.e. in the occurrence of stick–slip phenomena, where the inclusion of an event condition in the learning process proved to be a key feature of the framework. It is worth mentioning that, as shown in [13], providing known terms of the sought vector field in the form of a discrepancy bias, improved the accuracy of the method, yielding a generalizable EoM. When such a bias does not correspond to the true physics, even though a sufficient fitting of the data is observed, its generalizability is poor, as showcased when an ideal harmonic motion was provided for the experimental cases. Therefore, ongoing investigations are focusing on quantifying the various sources of uncertainty involved in PhI-SINDy, including the epistemic uncertainty due to a lack of knowledge about the correct physics bias.

Author contributions All authors contributed to the study conception and design. Material preparation, data collection and analysis were performed by Christos Lathourakis. The first draft of the manuscript was written by Christos Lathourakis and all authors commented on previous versions of the manuscript. All authors read and approved the final manuscript

Data Availibility The datasets generated during and/or analyzed during the current study, along with the Python scripts, are available in the GitHub repository https://github.com/xristosl0610/PhI-SINDy.

Declarations

Conflict of interest The authors have no relevant financial or non-financial interest to disclose.

References

1. Mendez, B., Botero, E., Romo, M.: A new friction law for sliding rigid blocks under cyclic loading. Soil Dyn. Earthq. Eng. **29**(5), 874–882 (2009)
2. Cabboi, A., Putelat, T., Woodhouse, J.: The frequency response of dynamic friction: enhanced rate-and-state models. J. Mech. Phys. Solids **92**, 210–236 (2016)
3. Green, P., Worden, K., Sims, N.: On the identification and modelling of friction in a randomly excited energy harvester. J. Sound Vib. **332**(19), 4696–4708 (2013)
4. Gutowski, P., Leus, M.: The effect of longitudinal tangential vibrations on friction and driving forces in sliding motion. Tribol. Int. **55**, 108–118 (2012)
5. Fehr, J., Kargl, A., Eschmann, H.: Identification of friction models for mpc-based control of a powercube serial robot. arXiv preprint arXiv:2203.10896 (2022)
6. Didonna, M., Stender, M., Papangelo, A., Fontanela, F., Ciavarella, M., Hoffmann, N.: Reconstruction of governing equations from vibration measurements for geometrically nonlinear systems. Lubricants **7**(8), 64 (2019)
7. Ren, Y., Adams, C., Melz, T.: Uncertainty analysis and experimental validation of identifying the governing equation of an oscillator using sparse regression. Appl. Sci. **12**(2), 747 (2022)
8. Brunton, S.L., Proctor, J.L., Kutz, J.N.: Discovering governing equations from data by sparse identification of nonlinear dynamical systems. Proc. Natl. Acad. Sci. **113**(15), 3932–3937 (2016)
9. Cabboi, A., Marino, L., Cicirello, A.: A comparative study between amontons-coulomb and dieterich-ruina friction laws for the cyclic response of a single degree of freedom system. Eur. J. Mech.-A/Solids **96**, 104737 (2022)
10. Marino, L., Cicirello, A.: A switching gaussian process latent force model for the identification of mechanical systems with a discontinuous nonlinearity. Data-Centr. Eng. **4**, e18 (2023)
11. Mahajan, S., Cicirello, A.: Governing equation identification of nonlinear single degree-of-freedom oscillators with coulomb friction using explicit stick and slip temporal constraints. ASCE-ASME J. Risk Uncert. Eng. Syst. Part B Mech. Eng. **9**(4) (2023)
12. Goyal, P., Benner, P.: Discovery of nonlinear dynamical systems using a runge-kutta inspired dictionary-based sparse regression approach. Proc. R. Soc. A **478**(2262), 20210883 (2022)
13. Lathourakis, C., Cicirello, A.. Physics-enhanced sparse identification of nonlinear oscillator with coulomb friction. In: Lacarbonara, W. (eds.) Advances in Nonlinear Dynamics, Volume III. ICNDA 2023. NODYCON Conference Proceedings Series. Springer, Cham (2024)
14. Karniadakis, G.E., Kevrekidis, I.G., Lu, L., Perdikaris, P., Wang, S., Yang, L.: Physics-informed machine learning. Nat. Rev. Phys. **3**(6), 422–440 (2021)
15. Schmidt, M., Lipson, H.: Distilling free-form natural laws from experimental data. Science **324**(5923), 81–85 (2009)
16. Dieterich, J.H.: Modeling of rock friction: 1. Experimental results and constitutive equations. J. Geophys. Res. Solid Earth **84**(B5), 2161–2168 (1979)
17. Rice, J.R., Ben-Zion, Y.: Slip complexity in earthquake fault models. Proc. Natl. Acad. Sci. **93**(9), 3811–3818 (1996)
18. Hasselmann, K., Barnett, T.P., Bouws, E., Carlson, H., Cartwright, D.E., Enke, K., Ewing, J., Gienapp, A., Hasselmann, D., Kruseman, P., et al.: Measurements of wind-wave growth and swell decay during the joint north sea wave project (jonswap). Ergaenzungsheft zur Deutschen Hydrographischen Zeitschrift, Reihe A (1973)
19. Hastie, T., Tibshirani, R., Friedman, J.H., Friedman, J.H.: The Elements of Statistical Learning: Data Mining, Inference, and Prediction, vol. 2. Springer, New York (2009)

20. Tibshirani, R.: Regression shrinkage and selection via the lasso. J. Roy. Stat. Soc. Ser. B (Methodol.) **58**(1), 267–288 (1996)
21. Marino, L., Cicirello, A.: Experimental investigation of a single-degree-of-freedom system with coulomb friction. Nonlinear Dyn. **99**(3), 1781–1799 (2020)
22. Dormand, J.R., Prince, P.J.: A family of embedded runge-kutta formulae. J. Comput. Appl. Math. **6**(1), 19–26 (1980)
23. Putelat, T., Dawes, J.H., Willis, J.R.: Sliding modes of two interacting frictional interfaces. J. Mech. Phys. Solids **55**(10), 2073–2105 (2007)
24. Corbetta, M.: Application of sparse identification of nonlinear dynamics for physics-informed learning. In: Proceeding of 2020 IEEE Aerospace Conference, pp. 1–8. (2020)
25. Vazirizade, S.M.: An intelligent integrated method for reliability estimation of offshore structures wave loading applied in time domain. Ph.D. thesis, The University of Arizona (2019)